AD-A120 821 LINEAR THEORY OF THE E X B INSTABILITY WITH AN INHOMOGENEOUS FIELD(U) NAVAL RESEARCH LAB WASHINGTON DC J D HUBA ET AL. 13 OCT 82 NRL-MR-4901 1/1

UNCLASSIFIED F/G 20/3 NL

END

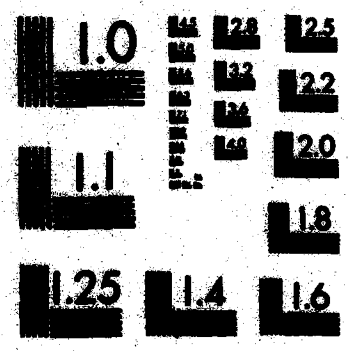
1.0
2.8
2.5
3.2
2.2
3.6
4.0
2.0
1.1
1.8
1.25
1.4
1.6

AD A120821

LABORATORY

D.C.

82 10 28 041

SECURITY CLASSIFICATION OF THIS PAGE (When Data Entered)

REPORT DOCUMENTATION PAGE

READ INSTRUCTIONS BEFORE COMPLETING FORM

1. REPORT NUMBER NRL Memorandum Report 4901	2. GOVT ACCESSION NO. AD-A120 821	3. RECIPIENT'S CATALOG NUMBER
4. TITLE (and Subtitle) LINEAR THEORY OF THE $E \times B$ INSTABILITY WITH AN INHOMOGENEOUS ELECTRIC FIELD		5. TYPE OF REPORT & PERIOD COVERED Interim report on a continuing NRL problem.
		6. PERFORMING ORG. REPORT NUMBER
7. AUTHOR(s) J.D. Huba, S.L. Ossakow, P. Satyanarayana*, and P.N. Guzdar**		8. CONTRACT OR GRANT NUMBER(s)
9. PERFORMING ORGANIZATION NAME AND ADDRESS Naval Research Laboratory Washington, DC 20375		10. PROGRAM ELEMENT, PROJECT, TASK AREA & WORK UNIT NUMBERS 62715H; 61153N; RR033-02-44; 47-0889-0-2; 47-0883-0-2
11. CONTROLLING OFFICE NAME AND ADDRESS Office of Naval Research, Arlington, VA 22217 Defense Nuclear Agency, Washington, DC 20305		12. REPORT DATE October 13, 1982
		13. NUMBER OF PAGES 55
14. MONITORING AGENCY NAME & ADDRESS(if different from Controlling Office)		15. SECURITY CLASS. (of this report) UNCLASSIFIED
		15a. DECLASSIFICATION/DOWNGRADING SCHEDULE

16. DISTRIBUTION STATEMENT (of this Report)

Approved for public release; distribution unlimited.

17. DISTRIBUTION STATEMENT (of the abstract entered in Block 20, if different from Report)

18. SUPPLEMENTARY NOTES

*Present address: Berkeley Scholars, Inc., Springfield, VA 22150
**Present address: Science Applications, Inc., McLean, VA 22102
(Permanent address: University of Maryland, College Park, MD 20742) (Continues)

19. KEY WORDS (Continue on reverse side if necessary and identify by block number)

$E \times B$ instability
Barium cloud striations
High-latitude F region irregularities
Velocity shear
Long wavelength selecuvity

20. ABSTRACT (Continue on reverse side if necessary and identify by block number)

A general linear theory of the $E \times B$ instability is developed which considers an ambient electric field that is at an arbitrary angle to the density gradient, and allows the electric field component parallel to the density gradient to be inhomogeneous. A differential equation is derived which describes the mode structure of the unstable waves in the direction of the inhomogeneities. The theory (1) includes ion inertia effects; (2) allows for arbitrary density and electric field profiles; and (3) is valid in the long wavelength regime, i.e., $k_y L < 1$ where L is the width of the boundary layer. The main results (Continues)

k small

DD FORM 1 JAN 73 1473 EDITION OF 1 NOV 65 IS OBSOLETE
S/N 0102-014-6601

SECURITY CLASSIFICATION OF THIS PAGE (When Data Entered)

18. Supplementary Notes (Continued)

This work was partially sponsored by the Defense Nuclear Agency under Subtask S99QAXHC, work unit 00082, work unit title "Plasma Structure Evolution," and by the Office of Naval Research.

20. Abstract (Continued)

V sub y

of the analysis are as follows. First, the inhomogeneous velocity flow caused by the inhomogeneous electric field can stabilize the instability. Second, short wavelength modes are preferentially stabilized over longer wavelength modes. Third, the stabilization mechanism is associated with the x dependent, Doppler-shifted frequency $\omega - k_y V_y(x)$ where $V_y(x) = -cE_x(x)/B$, ~~and not velocity shear terms proportional to $\partial V_y/\partial x$ or $\partial^2 V_y/\partial x^2$~~. And fourth, the marginal stability criterion is weakly dependent on the magnitude of ν_{in}/ω. Applications of these results to ionospheric phenomena are discussed, viz., barium cloud striations and high latitude F region irregularities.

omega - K sub y V sub y (x)

nu(in)/omega

Accession For	
NTIS GRA&I	☒
DTIC TAB	☐
Unannounced	☐
Justification	
By	
Distribution/	
Availability Codes	
Dist	Avail and/or Special
A	

CONTENTS

LINEAR THEORY OF THE E × B INSTABILITY WITH AN INHOMOGENEOUS ELECTRIC FIELD

I. INTRODUCTION

An important instability associated with the structuring of ionospheric plasmas (e.g., high latitude F region and barium clouds) is the $\underset{\sim}{E} \times \underset{\sim}{B}$ instability, also known as the gradient drift instability. The instability is an interchange instability which can occur in an inhomogeneous, weakly collisional, magnetized plasma that contains an ambient electric field orthogonal to both the ambient magnetic field and the density gradient. A simple physical picture of the instability mechanism is shown in Fig. 1. We consider a plasma such that $\underset{\sim}{B} = B\,\hat{e}_z$, $\underset{\sim}{E} = E\,\hat{e}_y$, $n = n(x)$ with $\partial n/\partial x > 0$ and $\nu_{en}/\Omega_e \ll \nu_{in}/\Omega_i \ll 1$ where $\nu_{\alpha n}$ is the collision frequency between species α and neutrals, and Ω_α is the cyclotron frequency of species α. Upon this plasma we impose a density perturbation $\delta n \sim \delta n \sin(k_y y)$ as shown in Fig. 1. The influence of $\underset{\sim}{E}$ on the plasma is to cause (1) the electrons and ions to $\underset{\sim}{E} \times \underset{\sim}{B}$ drift in the x direction and (2) an ion Pedersen drift in the y direction. The latter effect induces a space charge perturbation electric field denoted by $\delta\underset{\sim}{E}$. The response of the plasma to this perturbed electric field is to drift with a velocity $\delta\underset{\sim}{V} = c\delta\underset{\sim}{E} \times \underset{\sim}{B}/B^2$. For the configuration shown in Fig. 1, $\delta\underset{\sim}{V}$ causes the "heavy" fluid perturbation to fall into the "light" fluid (region I), and the "light" fluid perturbation to rise into the "heavy" fluid (region II) - the classic interchange phenomenon. Of course, if the direction of $\partial n/\partial x$ or E_y were reversed then the density perturbation would be damped.

The original study of the $\underset{\sim}{E} \times \underset{\sim}{B}$ instability was by Simon (1963) and Hoh (1963), who applied it to laboratory gas discharge experiments. Subsequent to these first investigations, a considerable amount of

Manuscript submitted July 8, 1982.

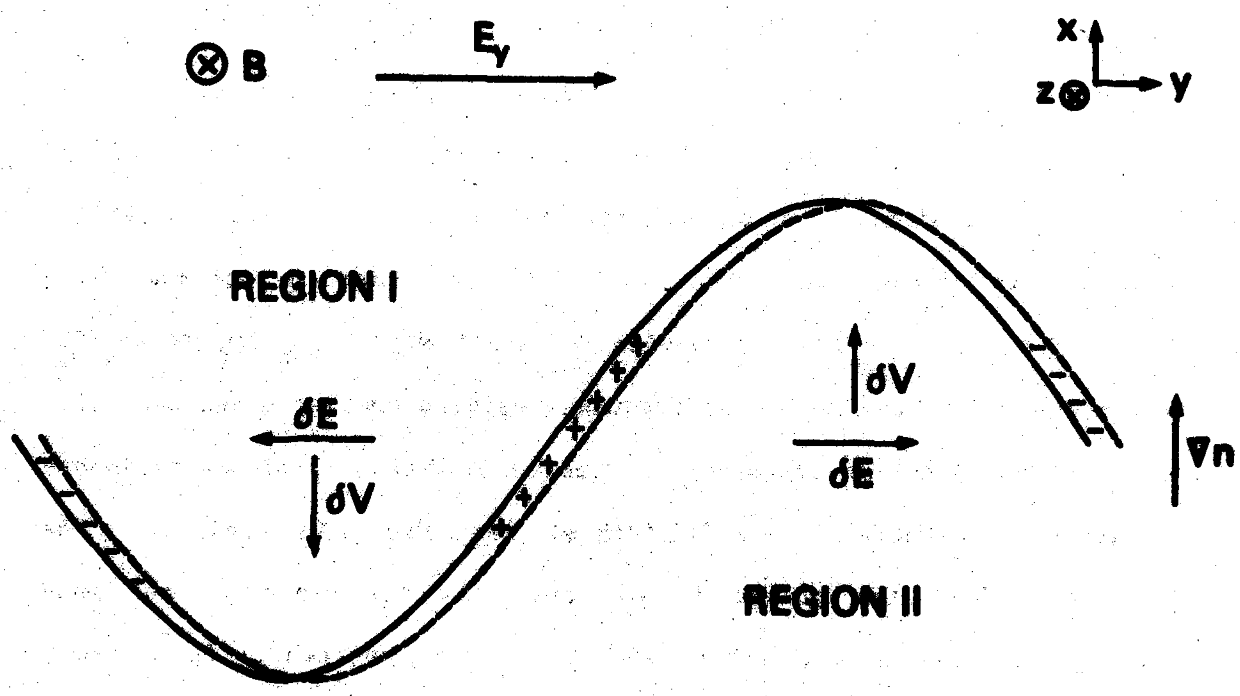

Fig. 1 Schematic of the physical mechanism of the $\underset{\sim}{E} \times \underset{\sim}{B}$ instability.

research has been devoted to explaining ionospheric phenomena based upon this instability (Linson and Workman, 1970 and references therein; Simon, 1970; Völk and Haerendel, 1971; Perkins et al., 1973; Zabusky et al., 1973; Shiau and Simon, 1972; Perkins and Doles, 1975; Scannapieco et al., 1976; Chaturvedi and Ossakow, 1979; Keskinen and Ossakow, 1982). Two areas of present interest concerning the instability are barium cloud striations (see for example the review papers Ossakow (1979) and Ossakow et al. (1982), and the references therein) and the structuring of plasma "blobs" in the high latitude F region (Vickrey et al., 1980; Keskinen and Ossakow, 1982).

The purpose of this paper is to present a general theory of the $\underset{\sim}{E} \times \underset{\sim}{B}$ instability which considers an ambient electric field at an arbitrary angle to the density gradient, and allows the electric field component parallel to the density gradient to be inhomogeneous. Some aspects of the problem have been treated by Perkins et al. (1973) and Perkins and Doles (1975). Perkins and Doles (1975) made the important discovery that the sheared velocity flow (resulting from an inhomogeneous electric field parallel to the density gradient) can stabilize the instability. Furthermore, short wavelength modes are preferentially stabilized over longer wavelength modes. The work of Perkins and Doles (1975) considered the strong collision limit ($\nu_{in} \gg \omega$), assumed a specific density profile amenable to analytical theory, and is valid only in the short wavelength regime, i.e., $k_y L \gg 1$ where L is the scale length of the boundary layer. The present study extends the theory of Perkins and Doles (1975) by removing these restrictions. Namely, we derive a differential equation which describes the mode structure of the $\underset{\sim}{E} \times \underset{\sim}{B}$ instability. Ion inertia effects are included so that the ratio ν_{in}/ω is arbitrary. Moreover, we solve this equation numerically so that arbitrary density and electric field profiles can be considered, and the regime $k_y L < 1$ can be investigated self-consistently.

The principal results of this work are the following.

1. The basic conclusions of Perkins and Doles (1975) are verified numerically. Specifically, the marginal stability criterion they derive analytically agrees well with our numerical result.

2. The marginal stability criterion is weakly dependent upon the magnitude of ν_{in}/ω.

3. The stabilization mechanism is associated with the x dependent, Doppler-shifted frequency $\omega - k_y V_y(x)$, where $V_y(x) = - cE_x(x)/B$, and not velocity shear terms proportional to $\partial V_y/\partial x$ or $\partial^2 V_y/\partial x^2$.

4. When $E_x(x_o) \gtrsim E_y$, where x_o is the position about which the mode is localized, the most unstable modes have $k_y L \lesssim 1$.

The organization of the paper is as follows. In Section II we derive the mode structure equation for the $\underset{\sim}{E} \times \underset{\sim}{B}$ instability. In Section III we present both analytical and numerical results based upon this equation. Finally, in Section IV we summarize our results and discuss applications to ionopheric phenomena, i.e., barium cloud striations and high latitude F region irregularities.

II. THEORY

The equilibrium configuration used in the analysis is shown in Fig. 2. The ambient magnetic and electric fields are in the z direction and the xy plane, respectively, where $\underset{\sim}{B} = B\, \hat{e}_z$ and $\underset{\sim}{E} = E_x(x)\, \hat{e}_x + E_y\, \hat{e}_y$. The electric field in the y direction is constant, while the electric field in the x direction is allowed to be a function of x. This gives rise to an inhomogeneous velocity flow in the y direction, i.e., $V_y(x) = -cE_x(x)/B$. The density is taken to be inhomogeneous in the x direction ($n = n(x)$) and temperature effects are ignored.

The basic assumptions used in the analysis are as follows. We assume that the perturbed quantities vary as $\delta p \sim \delta p(x) \exp\,[i(k_y y - \omega t)]$, where k_y is the wave number along y direction and $\omega = \omega_r + i\gamma$, implying growth for $\gamma > 0$. The ordering in the frequencies is such that $\omega \ll \Omega_i$ and $\nu_{in} \ll \Omega_i$ (the F region approximation), where ν_{in} is the ion-neutral collision frequency and Ω_i is the ion gyrofrequency. We neglect terms of order ω/Ω_i and ν_{in}/Ω_i, but retain terms of order ν_{in}/ω. We ignore finite gyroradius effects by limiting the wavelength domain to $kr_{Li} \ll 1$, where r_{Li} is the mean ion Larmor radius. We neglect perturbations along the magnetic field ($k_\parallel = 0$) so that only the two-dimensional mode structure in the xy plane is obtained. We retain ion inertial effects, thereby including the ion polarization drift, but ignore electron inertia.

A key feature of our analysis is that a nonlocal theory is developed. That is, the mode structure of the potential in the x direction, the direction in which density and the flow velocity are assumed to vary, is determined by a differential equation rather than an algebraic equation obtained by Fourier analysis. This is crucial to the

analysis since Perkins and Doles (1975) have shown that a nonlocal analysis is necessary to demonstrate the stabilizing influence of velocity shear, due to the inhomogeneous electric field parallel to the density gradient.

The fundamental equations used in the analysis are continuity and momentum transfer:

$$\frac{\partial n_\alpha}{\partial t} + \nabla \cdot (n_\alpha \underset{\sim}{V}_\alpha) = 0 \tag{1}$$

$$0 = -\frac{e}{m_e} (\underset{\sim}{E} + \frac{1}{c} \underset{\sim}{V}_e \times \underset{\sim}{B}) \tag{2}$$

$$\left(\frac{\partial}{\partial t} + \underset{\sim}{V}_i \cdot \nabla\right) \underset{\sim}{V}_i = \frac{e}{m_i} (\underset{\sim}{E} + \frac{1}{c} \underset{\sim}{V}_i \times \underset{\sim}{B}) - \nu_{in} \underset{\sim}{V}_i \tag{3}$$

where α denotes species (e: electrons, i: ions) and other variables have their usual meaning. Note that electron inertia terms are neglected, but ion inertia terms are included, and that the neutral wind is assumed to be zero. The equilibrium drifts are

$$\underset{\sim}{V}_e = - cE_x(x)/B \; \hat{e}_y \tag{4}$$

$$\underset{\sim}{V}_i = \left((\nu_{in}/\Omega_i)\; cE_x(x)/B + (cE_x'(x)/B\Omega_i)\; cE_y/B\right) \hat{e}_x$$

$$+ \left(-cE_x(x)/B + (\nu_{in}/\Omega_i)\; cE_y/B\right) \hat{e}_y \tag{5}$$

where we have chosen a reference frame such that $V_x = V_x - cE_y/B$, $\Omega_i = eB/m_i c$ and $E_x'(x) = \partial E_x/\partial x$. A relationship between n(x) and $E_x(x)$ can be derived by assuming $\nabla \cdot \underset{\sim}{J} = \nabla \cdot [n(\underset{\sim}{V}_i - \underset{\sim}{V}_e)] = 0$ which reduces to

$$\nabla \cdot (n\, \underset{\sim}{V}_i) = 0 \tag{6}$$

Equation (6) leads to

$$n(x)\, \left[(\nu_{in}/\Omega_i)\, cE_x(x)/B + (cE_x'(x)/B\Omega_i)\, cE_y/B \right] = \text{constant} \tag{7}$$

where we take the constant to be the LHS of Eq. (7) evaluated at $x = -\infty$. Thus, by specifying the density profile, the electric field profile $E_x(x)$ can be determined from Eq. (7). Of course, if there are sources and/or sinks in the plasma such that $\nabla \cdot (n\, \underset{\sim}{V}_i) \neq 0$, then Eq. (7) is not applicable.

We now consider a linear perturbation analysis of Eqs. (1)-(3). We assume $n_\alpha = n_\alpha + \delta n_\alpha$, $\underset{\sim}{V}_\alpha = \underset{\sim}{V}_\alpha + \delta \underset{\sim}{V}_\alpha$ and $\underset{\sim}{E} = \underset{\sim}{E} - \nabla\phi$ where ϕ is the perturbed electrostatic potential. Using Eqs. (2) and (3), we obtain

$$\delta V_{ex} = -\, ik_y \phi\, (c/B) \tag{8}$$

$$\delta V_{ey} = \phi'\, (c/B) \tag{9}$$

$$\delta V_{ix} = \left(-ik_y(1 - V_{iy}'/\Omega_i)\, \phi + i(\overline{\omega}/\Omega_i)\, \phi' - (V_{ix}/\Omega_i)\, \phi'' \right) (c/B) \tag{10}$$

$$\delta V_{iy} = \left(-k_y(\overline{\omega}/\Omega_i + i\, V_{ix}'/\Omega_i)\, \phi + (1 - ik_y V_{ix}/\Omega_i)\, \phi' \right) (c/B) \tag{11}$$

where $\overline{\omega} = \omega + i\nu_{in} - k_y V_{iy}$, $V_{iy}' = \partial V_{iy}/\partial x$, $V_{ix}' = \partial V_{ix}/\partial x$, $\phi' = \partial\phi/\partial x$ and $\phi'' = \partial^2\phi/\partial x^2$. Substituting Eqs. (8) - (11) into Eq (1), one can show that for the ions

$$-\frac{B}{c}\frac{\Omega_i}{\bar{\omega}}\left(\omega^*\frac{\delta n_i}{n} + iV_{ix}\frac{\delta n_i'}{n}\right) + i\frac{V_{ix}}{\bar{\omega}}\phi''' + \left(1 + i\frac{n'}{n}\frac{V_{ix}}{\bar{\omega}}\right)\phi''$$

$$+ \left(-ik_y^2\frac{V_{ix}}{\bar{\omega}} + \frac{n'}{n} + i\frac{V_{ix}}{\Omega_i}\left(\frac{n'}{n}\right)'\right)\phi' + \left(-k_y^2\left(1 + \frac{V_{ix}}{\bar{\omega}}\right) + \frac{k_y V_{iy}''}{\bar{\omega}}\right. \tag{12}$$

$$\left. + \frac{n'}{n}\frac{k_y V_{iy}'}{\bar{\omega}} - \frac{n'}{n}\frac{k_y \Omega_i}{\bar{\omega}}\right)\phi = 0$$

and for the electrons

$$\frac{\delta n_e}{n} = -\frac{c}{B}\frac{k\phi}{(\omega - k_y V_{ey})}\frac{n'}{n} \tag{13}$$

where $\omega^* = \omega - k_y V_{iy} + iV_{ix}'$ and the superscripts $(',{''},{'''})$ indicate first, second and third derivatives with respect to x, respectively.

We assume quasineutrality and take $\delta n_e = \delta n_i$. The following equation is then obtained from Eqs. (12) and (13),

$$i\frac{V_{ix}}{\bar{\omega}}\phi''' + \left(1 + i\frac{n'}{n}\frac{V_{ix}}{\bar{\omega}}\right)\phi'' + \left(\frac{n'}{n} + i\frac{k_y V_{ix}}{\bar{\omega}}\left(-k_y + \frac{\bar{\omega}}{\Omega_i}\frac{1}{k_y}\left(\frac{n'}{n}\right)'\right.\right.$$

$$\left.\left. + \frac{\Omega_i}{\omega - k_y V_{ey}}\frac{n'}{n}\right)\right)\phi' + \left(-k_y^2\left(1 + \frac{V_{ix}'}{\bar{\omega}}\right) + \frac{k_y V_{iy}''}{\bar{\omega}} + \frac{n'}{n}\frac{k_y V_{iy}'}{\bar{\omega}}\right.$$

$$+ i\frac{k_y V_{ix}}{\omega - k_y V_{ey}}\frac{\Omega_i}{\bar{\omega}}\frac{n''}{n} - i\frac{k_y V_{ey}'}{\omega - k_y V_{ey}}\frac{n'}{n}\frac{\nu_{in}}{\bar{\omega}}\frac{\omega}{\omega - k_y V_{ey}}$$

$$\left. - \frac{\nu_{in}}{\bar{\omega}}\frac{n'}{n}\frac{k_y}{\omega - k_y V_{ey}}k_y(cE_y/B)\right)\phi = 0 \tag{14}$$

We simplify Eq. (14) by assuming the following ordering scheme: $\partial/\partial x < k_y$, $\nu_{in}/\Omega_i \ll 1$, $V' \approx V/L$, $V'' \approx V/L^2$, $k_y L \ll \Omega_i/\nu_{in}$, $k_y L \ll \Omega_i/\omega$ where L is the scale length of the inhomogeneous plasma boundary layer. Equation (14) can now be written as

$$\phi'' + \left(\frac{n'}{n}\left(1 - \frac{i\nu_{in}}{\tilde{\omega}} \frac{k_y V_{ey}}{\tilde{\omega}+i\nu_{in}}\right)\right) \phi'$$

$$+ \left(-k_y^2 - \frac{k_y(cE_y/B)}{\tilde{\omega}+i\nu_{in}} \frac{\nu_{in}}{\tilde{\omega}} \frac{k_y n'}{n} + \frac{n'}{n} \frac{k_y V'_{ey}}{\tilde{\omega}+i\nu_{in}}\right.$$

$$\left. - \frac{k_y V_{ey}}{\tilde{\omega}+i\nu_{in}} \frac{i\nu_{in}}{\tilde{\omega}} \left(\frac{n''}{n} + \frac{V'_{ey}}{V_{ey}} \frac{n'}{n} \frac{\omega}{\tilde{\omega}}\right)\right) \phi = 0 \tag{15}$$

where $\tilde{\omega} = \omega - k_y V_{ey}(x) = \omega + k_y(cE_x(x)/B)$. Equation (15) describes the two-dimensional mode structure of ϕ for the $\underset{\sim}{E} \times \underset{\sim}{B}$ instability in a velocity sheared plasma for arbitrary ν_{in}/ω.

III. RESULTS

A. Analytical Results

In general, Eq. (15) requires a numerical analysis for arbitrary density and electric field profiles. However, insight into the nature of the $\underset{\sim}{E} \times \underset{\sim}{B}$ instability can be gained by first considering several limiting cases.

1. Local Theory

We first reduce the differential equation, Eq. (15), to an albegraic equation by making use of local theory. That is, we let $\partial/\partial x \to ik_x$, and assume $k_x^2 L_n^2 \gg 1$ and $k_y^2 L_n^2 \gg 1$ where $L_n = (n'/n)^{-1}$ is the scale length of the density inhomogeneity evaluated at $x = x_o$. For simplicity, we also take $\underset{\sim}{E} = E_x \hat{e}_x + E_y \hat{e}_y$ = constant. In this limit, Eq. (15) becomes

$$k^2 L_n^2 + k_y L_n \frac{\nu_{in}}{\tilde{\omega}} \frac{\underset{\sim}{k} \cdot \underset{\sim}{E}\,(c/B)}{\tilde{\omega} + i\nu_{in}} = 0 \tag{16}$$

where $\tilde{\omega} = \omega - k_y V_{ey}$ and $V_{ey} = -cE_x/B$. Equation (16) has the solution

$$\tilde{\omega} = -i\frac{\nu_{in}}{2}\left[1 \mp \left(1 + 4\frac{k_y}{k}\frac{\underset{\sim}{k} \cdot \underset{\sim}{E}\,(c/B)}{\nu_{in}\, kL_n}\right)^{1/2}\right] \tag{17}$$

Instability occurs when

$$\frac{k_y}{k}\frac{\underset{\sim}{k} \cdot \underset{\sim}{E}}{kL_n} > 0. \tag{18}$$

The growth rates of the instability in the strong and weak collisional limits are, respectively,

$$\gamma = \frac{k_y}{k} \frac{\underset{\sim}{k} \cdot \underset{\sim}{E}\,(c/B)}{kL_n} \qquad ; \nu_{in} \gg \omega \tag{19}$$

$$\gamma = \frac{k_y}{k}\left(\frac{\underset{\sim}{k} \cdot \underset{\sim}{E}\,(c/B)}{kL_n}\,\nu_{in}\right)^{1/2} \qquad ; \nu_{in} \ll \omega \tag{20}$$

with a real frequency $\omega = k_y V_{ey}$ in each case. Note that instability can occur for $E_y = 0$ as long as $k_y \neq 0$ and $E_x \neq 0$ (Eq. (18); see also Keskinen and Ossakov (1982). For $k = k_y$, one obtains the usual $\underset{\sim}{E} \times \underset{\sim}{B}$ gradient drift instability growth rate (Linson and Workman, 1971) in Eq. (19), and the so-called high altitude limit (Ossakov et al., 1978) of the $\underset{\sim}{E} \times \underset{\sim}{B}$ gradient drift instability in Eq. (20).

2. Nonlocal Theory

In deriving Eq. (16) the local approximation is used. That is, the dispersion equation is solved based upon the plasma parameters at a particular value of x, say $x = x_o$; usually where n'/n is a maximum which leads to maximum growth. If we now assume $E_x = E_x(x)$ then a sheared E x B velocity flow arises $V_y = V_{ey}(x) = - cE_x(x)/B$. Applying local theory to this situation, one might expect that Eq. (16) is still valid with V_{ey} evaluated at x_o, i.e., $V_{ey} = V_{ey}(x_o)$. Thus, Eqs. (19) and (20) follow accordingly, but the real frequency is now given by $\omega_r = k_y V_{ey}(x_o)$. However, Perkins and Doles (1975) have shown, both analytically and using numerical simulations, that this is not the case. We do not reproduce their detailed analysis here, but rather, point out the important result of their work.

Perkins and Doles (1975) consider the strong collision limit ($\nu_{in} \gg \omega$) so that ion inertia terms can be neglected. Furthermore, they assume $\nabla \cdot (n \underline{V}) = 0$ which leads to

$$n(x)\, E_x(x) = n_o\, E_{ox} = \text{constant} \tag{21}$$

where $n_o = n(x = -\infty)$ and $E_{ox} = E_x(x = -\infty)$. This is evident from Eq. (7) by noting that $E_x'(x) \sim E_x/L_n$ and $\nu_{in} \gg \omega \sim cE_y/BL_n$. In this limit, Eq. (15) reduces to

$$\phi'' + [\frac{n'}{n}(1 - \frac{kV_{ey}}{\tilde{\omega}})]\,\phi'$$

$$+ [-k_y^2 + i\,\frac{k_y(cE_y/B)}{\tilde{\omega}}\,\frac{k_y n'}{n} - \frac{k_y V_{ey}}{\tilde{\omega}}(\frac{n''}{n} + \frac{V_{ey}'}{V_{ey}}\,\frac{n'}{n}\,\frac{\omega}{\tilde{\omega}})]\,\phi = 0 \tag{22}$$

where $\tilde{\omega} = \omega - k_y V_{ey}$, $V_{ey} = -(cE_{ox}/B)(n_o/n(x))$ and $V_{ey}' = -(cE_{ox}/B)(n_o/n(x))'$. Perkins and Doles (1975) expand Eq. (22) about $x = x_o$ where x_o is the position of maximum n'/n by taking

$$n'/n = [1-(x-x_o)^2/D^2]/L_n \tag{23}$$

Assuming $k_y^2 L_n^2 \gg 1$ and $k_y^2 D^2 \gg 1$, and by making several variable changes, they solve Eq. (22) analytically. The important conclusion of their theory is that is that the $\underline{E} \times \underline{B}$ instability is stabilized when

$$\frac{E_x(x_o)}{E_y} > \frac{2}{k_y D} \tag{24}$$

Thus, the influence of velocity shear, i.e., an inhomogeneous E_x, is to preferentially stabilize the short wavelength modes, those with $k_y D \gg 1$.

B. Numerical Results

In order to solve Eq. (15) numerically, and also to gain insight into the nature of the solutions, we transform Eq. (15). First, we note that Eq. (15) is of the form

$$\phi'' + p(x)\,\phi' + q(x)\,\phi = 0 \tag{25}$$

where p(x) and q(x) are the coefficients of ϕ' and ϕ, respectively, in Eq. (15). We let

$$\phi = \tilde{\phi}\,\exp(-1/2\int^{x} p(s)\,ds) \tag{26}$$

Substituting Eq. (26) into Eq. (25), we find that the transformed equation is

$$\tilde{\phi}'' - Q(x)\,\tilde{\phi} = 0 \tag{27}$$

where

$$Q(x) = -q(x) + 1/2\,p'(x) + 1/4\,(p(x))^2 \tag{28}$$

and

$$p(x) = \frac{n'}{n}\left(1 - \frac{i\nu_{in}}{\tilde{\omega}}\,\frac{k_y V_{ey}}{\tilde{\omega}+i\nu_{in}}\right) \tag{29}$$

$$p'(x) = \left(\frac{n''}{n} - \left(\frac{n'}{n}\right)^2\right)\left(1 - \frac{i\nu_{in}}{\tilde{\omega}}\,\frac{k_y V_{ey}}{\tilde{\omega}+i\nu_{in}}\right)$$

$$- \frac{n'}{n}\,\frac{k_y V'_{ey}}{\tilde{\omega}+i\nu_{in}}\,\frac{i\nu_{in}}{\tilde{\omega}}\left(1 + \frac{k_y V_{ey}}{\tilde{\omega}+i\nu_{in}} + \frac{k_y V_{ey}}{\tilde{\omega}}\right) \tag{30}$$

$$q(x) = -k_y^2 - \frac{k_y(cE_y/B)}{\tilde{\omega}+i\nu_{in}}\,\frac{\nu_{in}}{\tilde{\omega}}\,\frac{k_y n'}{n} + \frac{n'}{n}\,\frac{k_y V'_{ey}}{\tilde{\omega}+i\nu_{in}}$$

$$- \frac{k_y V_{ey}}{\tilde{\omega}+i\nu_{in}}\,\frac{i\nu_{in}}{\tilde{\omega}}\left(\frac{n''}{n} + \frac{V'_{ey}}{V_{ey}}\,\frac{n'}{n}\,\frac{\omega}{\tilde{\omega}}\right) \tag{31}$$

Equation (27) has a simple form, albeit $Q(x)$ is a complicated function of x, which allows physical insight into the nature of the mode structure. As an example, if Q is real and has $Q > 0$ for $|x| > x_o$ and $Q < 0$ for $|x| < x_o$ then one would expect a bounded solution of $\tilde{\phi}$ in the region $|x| < x_o$ that exponentially decays for $|x| > x_o$.

We now solve Eq. (27) numerically for a variety of conditions to better understand the influence of an inhomogeneous electric field on the $\underset{\sim}{E} \times \underset{\sim}{B}$ instability. In all of the cases presented, the following density profile is assumed

$$n(x) = n_o \; \frac{1 + \varepsilon \tanh (x/L)}{1 - \varepsilon} \tag{32}$$

where $0 < \varepsilon < 1$, L characterizes the width of the boundary layer, and $n_o = n\,(x = -\infty)$. By varying ε, the magnitude of the density gradient scale length L_n ($L_n = (n'/n)^{-1}$) can be changed. That is, as $\varepsilon \rightarrow 0$, $L_n \rightarrow \infty$ (a constant density profile); as $\varepsilon \rightarrow 1$, the value of $L_n \rightarrow 0$ (a rapidly changing density profile). We assume $\varepsilon = 0.95$ for the results presented so that

$$\left(\frac{n'}{n}\right)_{max} = 1.45\ L^{-1} \qquad \text{at } x/L = -\,0.9 \tag{33}$$

The maximum growth rate of the instability is expected to be

$$\gamma_m = 1.45\ (V_o/L) \tag{34}$$

where $V_o = cE_o/B$ and we have used Eq. (19) assuming $\underset{\sim}{E} = E_o\, \hat{e}_y$.

The ambient electric field is chosen to be

$$\underset{\sim}{E}(x) = E_x(x)\ \hat{e}_x + E_y\ \hat{e}_y \tag{35}$$

where

$$\underset{\sim}{E}\ (x = -\infty) = E_o \sin\theta\ \hat{e}_x + E_o \cos\theta\ \hat{e}_y \tag{36}$$

so that $\theta = \tan^{-1}(E_x/E_y)$ at $x = -\infty$. The influence of the x component of the electric field is then studied by varying θ , the angle between $\underset{\sim}{E}$ and $\hat{e}_y$ at $x = -\infty$. Two forms of $E_x(x)$ are considered in the analysis:

$$E_x(x) = E_o \sin\theta = \text{constant} \tag{37}$$

and

$$E_x(x) = E_o \sin\theta\ (n_o/n(x)) \neq \text{constant} \tag{38}$$

These allow us to contrast the effects of no velocity shear and velocity shear on the instability. We comment that Eq. (38) is an equilibrium solution which satisfies $\nabla \cdot (n\ \underset{\sim}{V}_i) = 0$ in the strong collisional limit $\nu_{in} >> \omega$ (i.e., Eq. (7)).

In Fig. 3 we plot $\tilde{\gamma} = \gamma/(V_o/L)$ vs k_yL for $\theta = 0^o$ and 90^o and $\tilde{\nu} = \nu/(V_o/L) = 1.0$ and 100.0, where E_x is chosen to be constant (Eq. (37)) and $V_o = cE_o/B$. A general comment on all of the curves shown is that $\tilde{\gamma}$ is an increasing function k_yL , but $\tilde{\gamma}$ asymptotes to a constant value independent of k_yL for $k_y^2\ L^2 >> 1$. This is consistent with the predictions of local theory. The "standard" case is $\theta = 0^o$, that is, $\underset{\sim}{E} = E_y\hat{e}_y$ and there is no component of $\underset{\sim}{E}$ parallel to the density gradient. For this case, two values of $\tilde{\nu}$ are chosen: strong collisions ($\tilde{\nu} = 100.0$) and weak

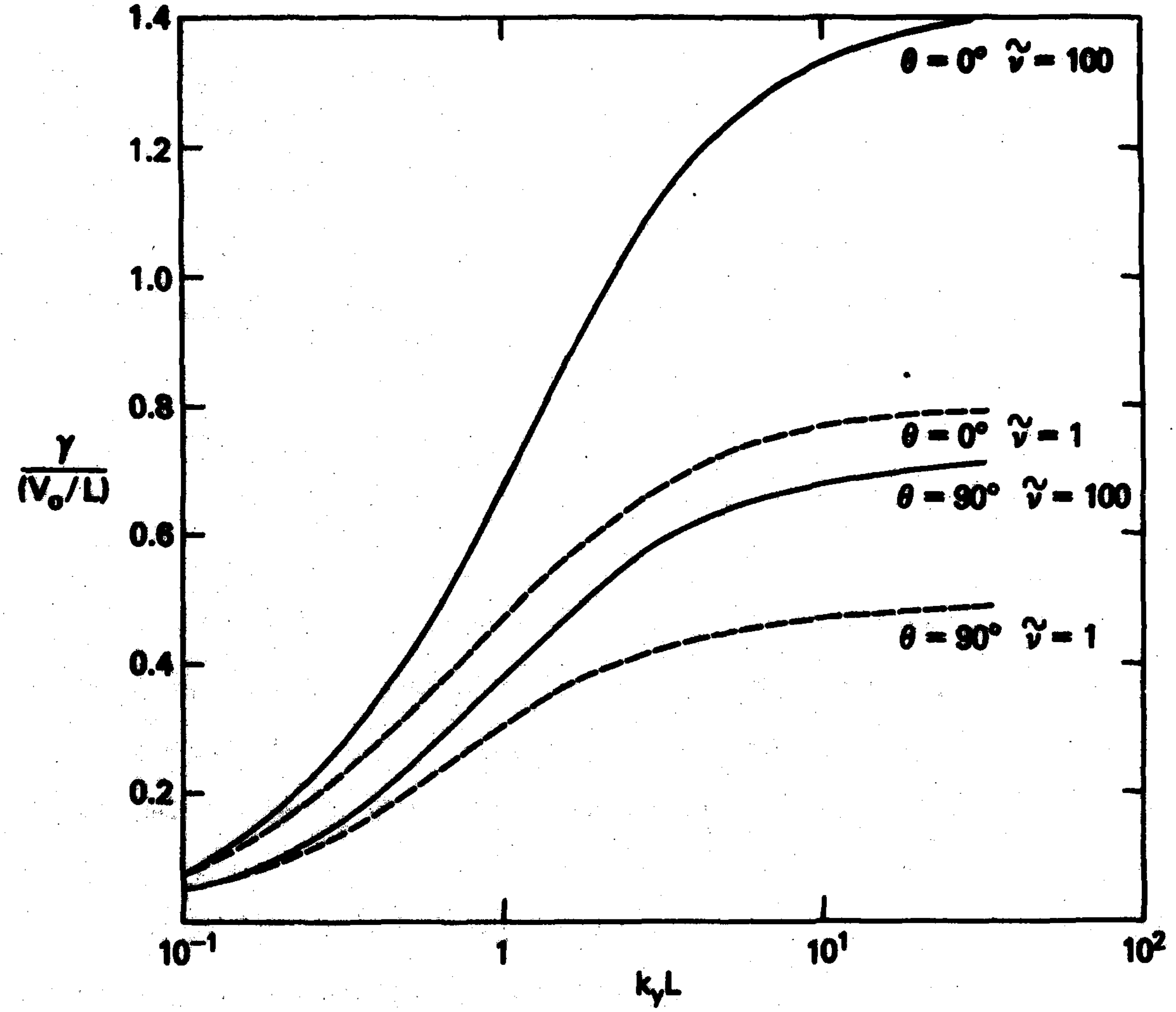

Fig. 3 Plot of $\tilde{\gamma} = \gamma/(V_o/L)$ vs. k_yL for $\theta = 0^o$ and 90^o, and for $\tilde{\nu} = \nu_{in}/(V_o/L) = 1.0$ and 100.0. The electric field E_x is assumed to be constant (Eq. (37)).

collisions ($\tilde{\nu} = 1.0$). As is expected, the growth rate is larger for the larger value of $\tilde{\nu}$ in the short wavelength regime ($k_y L > 1$). Also, the growth rate for $\tilde{\nu} = 100.0$ at $k_y L = 30$ is $\tilde{\gamma} = 1.39$, and is still increasing, although slowly, as a function of $k_y L$. This value of $\tilde{\gamma}$ agrees well with the value obtained from local theory ($\tilde{\gamma} = 1.45$ from Eq. (33)). The growth rate for the weak collision case $\tilde{\nu} = 1.0$ asymptotes to a somewhat smaller value of $\tilde{\gamma}$ ($\tilde{\gamma} = 0.79$). However, note that the difference between the growth rates for the strong and weak collisional cases becomes smaller as $k_y L \to 0$, and that the growth rates are, in fact, comparable for $k_y L \approx 0.1$. The "non-standard" case is $\theta = 90^\circ$, or $\underset{\sim}{E} = E_x \hat{e}_x$ and the only component of $\underset{\sim}{E}$ is along the density gradient. The major result of this limit is simply that the instability can still persist even though $E_y = 0$. The overall influences of $\tilde{\nu}$ and $k_y L$ on the instability are the same as in the previous case, $\theta = 90^\circ$.

In Fig. 4 we plot $\tilde{\gamma}$ vs. $k_y L$ for $\theta = 0^\circ$ and 70° and $\tilde{\nu} = 1.0$ and 100.0, but consider E_x to be a function of x as in Eq. (38) so that velocity sheared flows occur for $\theta \neq 0^\circ$. The curves for $\tilde{\nu} = 1.0$ and 100.0 and $\theta = 0^\circ$ are shown for comparative purposes. The important results in this figure are as follows. First, the mode is <u>stable</u> for $k_y L \gtrsim 12$ for both the strong and weak collisional cases when $\theta = 70^\circ$. This is in agreement with the conclusion of Perkins and Doles (1975); velocity shear effects tend to stabilize the short wavelength modes, those such that $k_y^2 L^2 \gg 1$. The influence of shear on the long wavelength modes ($k_y L < 1$) is weakly stabilizing. Second, the difference in the growth rate curves for $\tilde{\nu} = 1.0$ and 100.0 is much less than that of the case of no shear (i.e., $\theta = 0$). And finally, since velocity shear can stabilize short wavelength modes before long wavelength modes, velocity

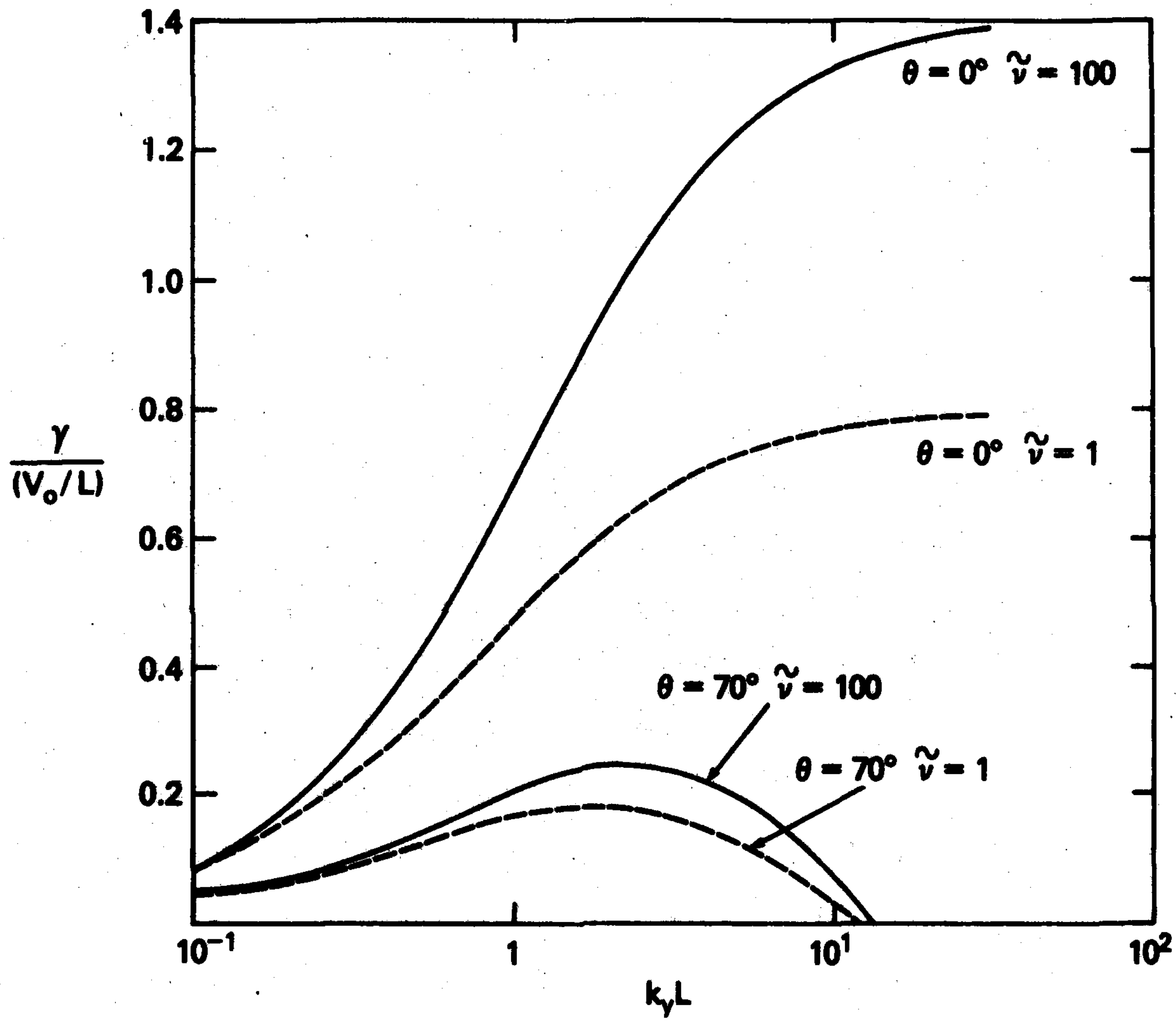

Fig. 4 Plot of $\tilde{\gamma} = \gamma/(V_o/L)$ vs. k_yL for $\theta = 0^o$ and 70^o, and for $\tilde{\nu} = \nu_{in}/(V_o/L) = 1.0$ and 100.0. The electric field E_x is assumed to be inhomogeneous (Eq. (38)).

[illegible] causes a preferential wavelength to be excited based upon linear theory. For the case where ($\theta = 70^\circ$), the linear growth maximizes at $k_y L \approx$ [illegible]. Thus, velocity shear can lead to growth of long wavelength modes ($k_y L \sim 1$), rather than short wavelength modes ($k_y L \gg 1$).

Figure 5 is a plot of γ vs. $k_y L$ for $\bar{V} = 100.0$ and $\theta = 0^\circ$, 10°, 30°, 50°, 70° and 80°. It is clear that a peak in the linear growth rate occurs because of velocity shear. Moreover, as θ increases, the position of maximum growth [illegible] as a function of $k_y L$. For $\theta = 10^\circ$ maximum growth occurs for $k_y L \approx$ [illegible] while for $\theta = 80^\circ$ maximum growth occurs for $k_y L \approx 1.0$.

To further illustrate the influence of velocity shear on the $E \times B$ instability we present Fig. 6 which is a plot of γ vs. θ for $\bar{V} = 100.0$, $k_y L = 1.0$ and 10.0, and γ found by using Eq. (27) and Eq. (28). Here, [illegible]

[illegible]

It is evident from the preceding discussion, an inhomogeneous [illegible] has a dramatic effect on the $E \times B$ instability. However, Eq. (27) is rather complicated and a question that naturally arises is, which term (or terms) in Eq. (27) is responsible for stabilization of the

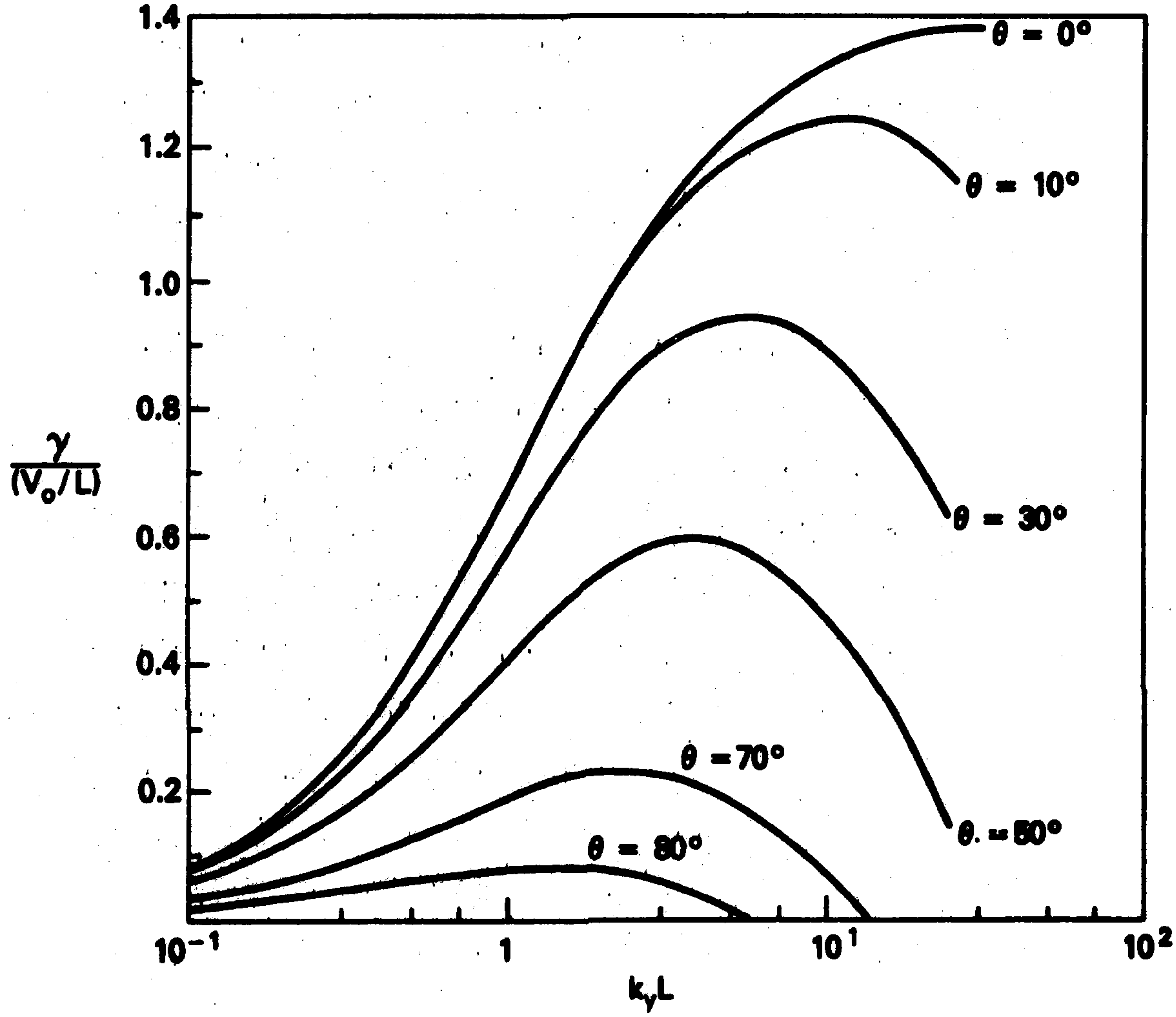

Fig. 5 Plot of $\tilde{\gamma} = \gamma/(V_o/L)$ vs. k_yL for $\tilde{\nu} = \nu_{in}/(V_o/L) = 100.0$ and $\theta = 0^o$, 10^o, 30^o, 50^o, 70^o and 80^o.

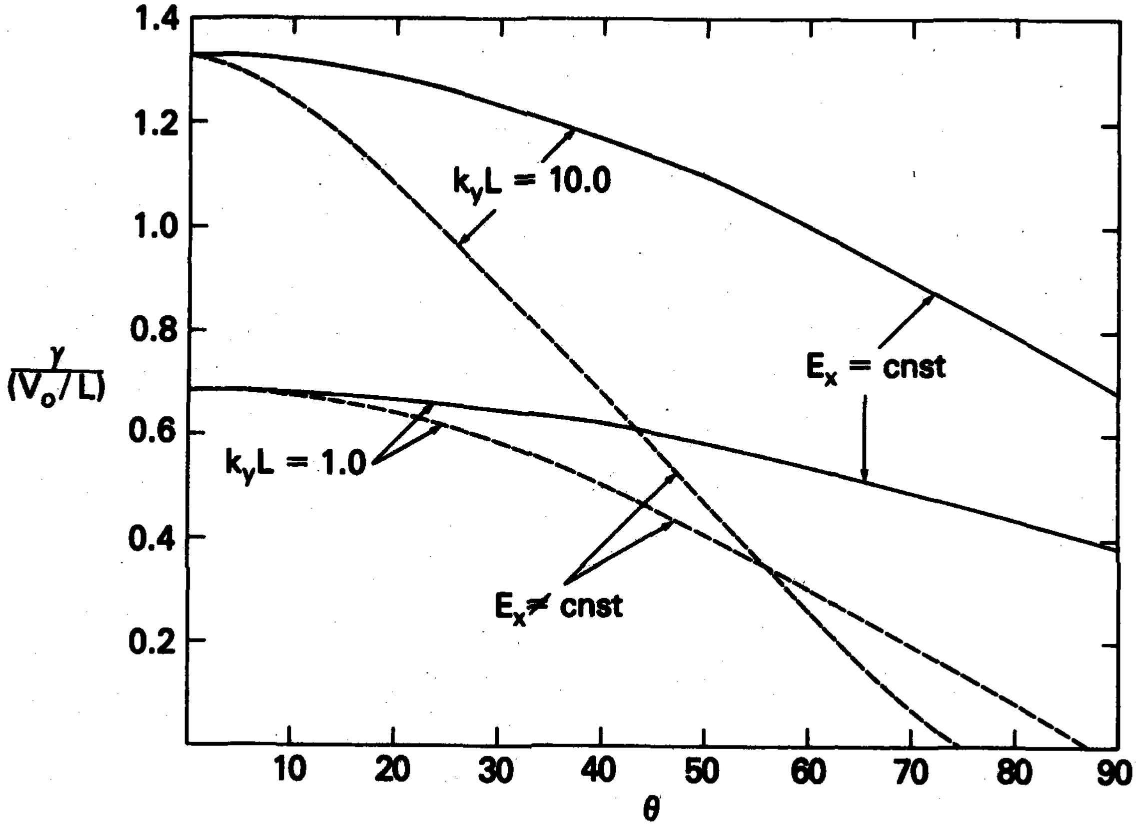

Fig. 6 Plot of $\tilde{\gamma} = \gamma/(V_o/L)$ vs θ for $\tilde{\gamma} = \gamma_{in}/(V_o/L) = 100.0$, $k_yL = 1.0$ and 10.0, and E_x = cnst (Eq. (37)) and $E_x \neq$ cnst (Eq. (38)).

mode? To shed light on this question, we consider the following simplified equation

$$\phi'' - [k_y^2 - ik_y \frac{k_y (cE_y/B)}{\omega - k_y V_{ey}(x)} \frac{n'}{n}] \phi = 0 \tag{39}$$

That is, we consider the limit $\tilde{\nu} \gg 1$ and retain the x-dependent, Doppler-shifted frequency $(\omega - k_y V_{ey}(x))$ as the only contribution of the inhomogeneous electric field profile. We neglect terms proportional to V'_{ey}, V''_{ey}, and n''. We emphasize that Eq. (39) is not the complete mode structure equation, but is solved and contrasted to the correct solution in order to isolate a single effect of the field inhomogeneity, viz., the x dependent resonance $\omega - k_y V_{ey}(x)$. In Fig. 7 we plot $\tilde{\gamma}$ vs. $k_y L$ for $\theta = 70^{\circ}$ and E_x is given by Eq. (38). The solid curve is the solution to Eq. (27) for $\tilde{\nu} = 100.0$, while the dashed curve is the solution to Eq. (39). Although there is a small difference between these curves for $k_y L < 1$, the important point is that the mode is stabilized at $k_y L \approx 13$ in both cases. Thus, the stabilization mechanism is related to the x dependent resonance $\omega - k_y V_{ey}(x)$, as opposed to velocity shear effects associated with terms proportional to V'_{ey} and V''_{ey}. This is a key result of this analysis.

We now turn our attention to the mode structure associated with the $\mathbf{E} \times \mathbf{B}$ instability, and the influence of an inhomogeneous electric field on its structure. Figure 8 is a plot of the density profile $n(x)/n_0$ (Eq. (32) with $\varepsilon = .095$) and the electric field profile $E_x(x)/E_{0x}$ (Eq. (38) with $E_{0x} = E_0 \sin\theta$) versus x/L. For $\theta = 0^{\circ}$, the electric field profile is simply $E_x(x)/E_{0x} = 0$. We present plots of Q and $\tilde{\phi}$ vs. x/L for these profiles. In the subsequent plots of Q and $\tilde{\phi}$, the subscript r denotes the

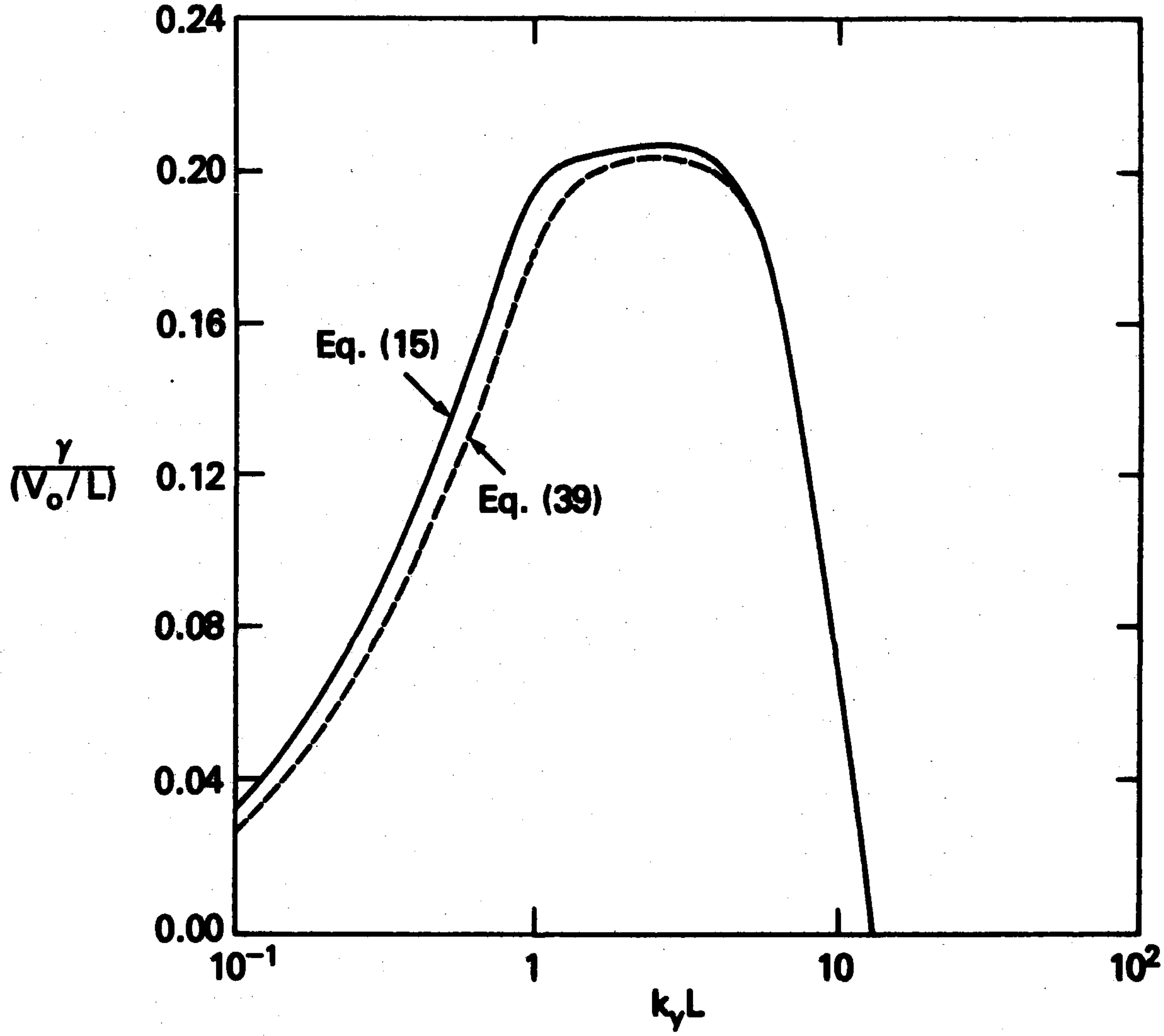

Fig. 7 Plot of $\tilde{\gamma} = \gamma/(V_o/L)$ vs k_yL for $\tilde{\nu} = \nu_{in}/(V_o/L) = 100.0$ and $\theta = 70^o$ using Eq. (27) (solid curve) and Eq. (39) (dashed curve). The electric field E_x is assumed to be inhomogeneous (Eq. (38)).

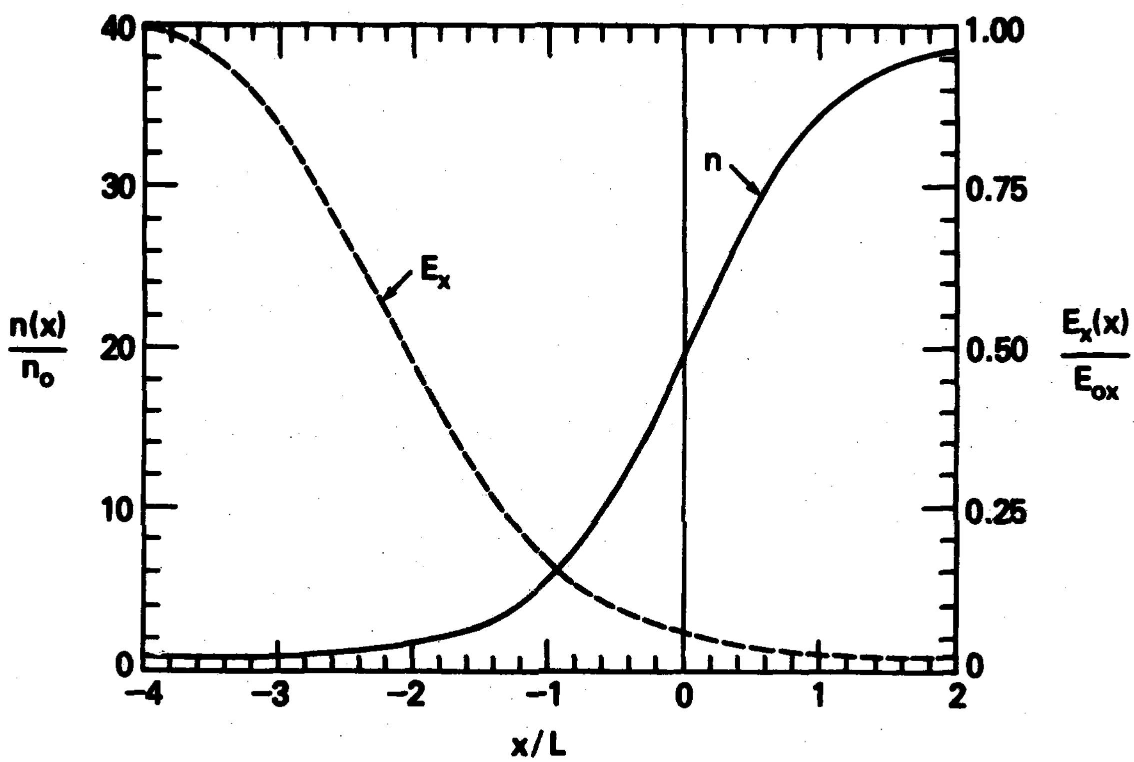

Fig. 8 Equilibrium density (Eq. (32)) and electric field (Eq. (38)) profiles for $\epsilon = 0.95$.

real part of Q or $\tilde{\phi}$, and i denotes the imaginary part of Q or $\tilde{\phi}$. The parameters considered for the first set of modes are k_yL = 10.0, $\tilde{\nu}$ = 100.0, and $\theta = 0^o$ (Fig. 9) and $\theta = 70^o$ (Fig. 10). These modes are considered to be short wavelength modes since $k_yL \gg 1$.

Figure 9 is a plot of Q (Fig. 9a) and $\tilde{\phi}$ (Fig. 9b) versus x/L for the case of no electric field inhomogeneity ($\theta = 0^o$ or $E_x(x) = 0$). the eigenfrequency for the mode is $\tilde{\omega}_r = 0.0$ and $\tilde{\gamma} = 1.329$. the important points to note are the following. First, the wave potential Q is real and is such that $Q < 0$ for $-1.3 < x/L < -0.5$ and $Q > 0$ otherwise. Second, the wave potential Q achieves a minimum at $x/L \approx -0.9$, the position of maximum L_n (Eq. (33)). Third, consistent with this form of Q, the wave function $\tilde{\phi}$ is a bounded mode centered about $x/L \approx -0.9$ that falls off exponentially for $x/L > -0.5$ and $x/L < -1.3$. And finally, the wave function is reasonably broad in that its half-width at half maximum (Δx) is comparable to the width of the boundary layer, i.e., $\Delta x \approx L/2$.

Figure 10 is a plot of Q (Fig. 10a) and $\tilde{\phi}$ (Fig. 10b) versus x/L for the case of an inhomogeneous electric field ($\theta = 70^o$ and $E_x(x)$ is shown in Fig. 8). The eigenfrequency for this case is $\tilde{\omega}_r = 0.5307$ and $\tilde{\gamma} = 0.0716$. Note that the mode has a real frequency in contrast to the previous case and that the growth rate is smaller. Other important differences between this situation and the previous one are as follows. First, the wave potential Q is shifted to a larger value of x/L. The position of the minimum value of Q_r is at $x/L \approx -0.12$. Also, note that Q also has an imaginary component. Second, the wave function $\tilde{\phi}$ is the lowest order mode and has considerably more structure in x/L than the no shear case. Finally, the spatial extent of $\tilde{\phi}$ is somewhat narrower with $\Delta x \approx 0.1$ L.

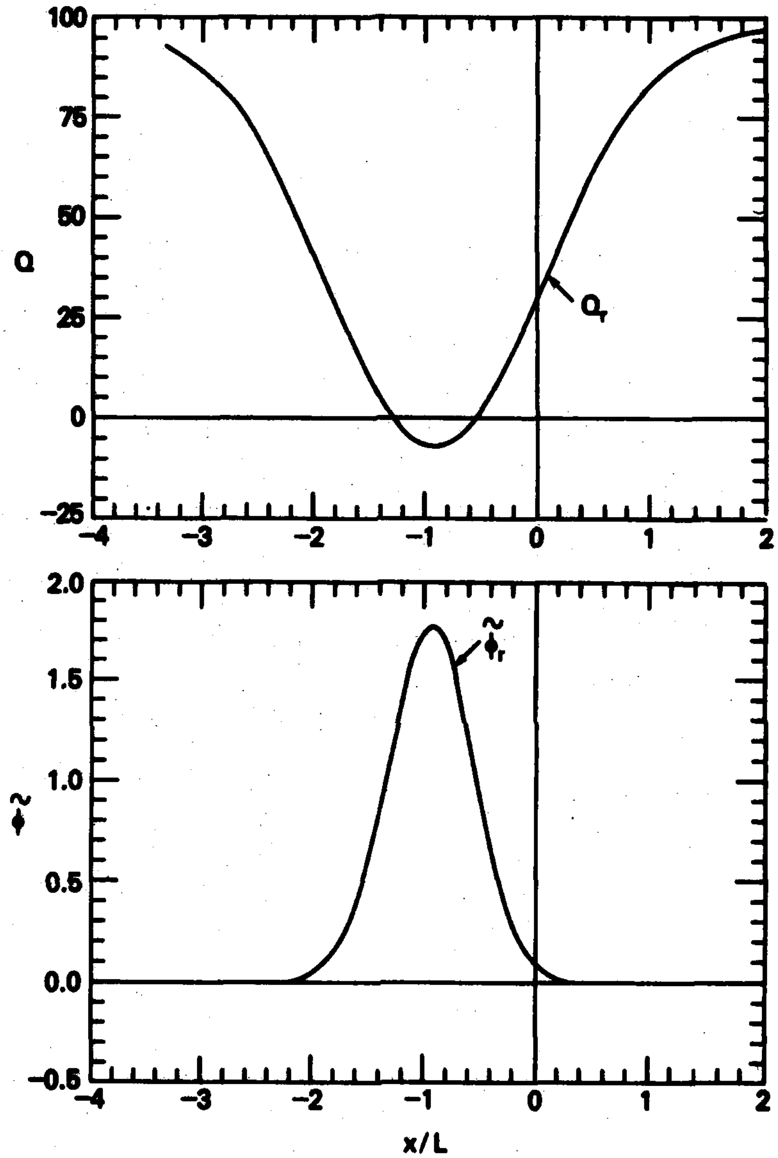

Fig. 9 Wave potential Q and wave eigenfunction $\tilde{\phi}$ as a function of x/L. The subscripts r and i denote real and imaginary, respectively. The parameters considered are $k_yL = 10.0$, $\tilde{\nu} = \nu_{in}/(V_o/L) = 100.0$ and $\theta = 0^o$ (i.e., $E_x = 0$). The eigenfrequency is $\tilde{\omega}_r = 0.0$ and $\tilde{\gamma} = 1.329$. (a) Q vs. x/L. (b) $\tilde{\phi}$ vs. x/L.

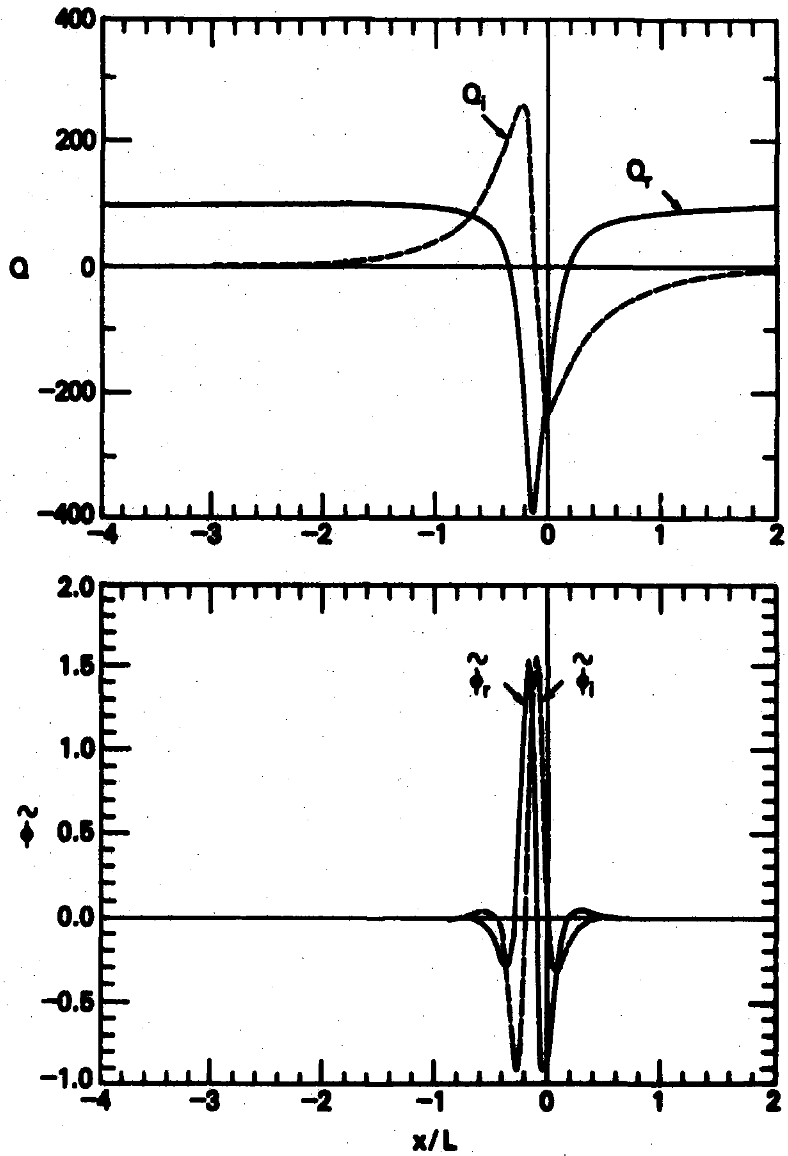

Fig. 10 Wave potential Q and wave eigenfunction as a function of x/L. The subscripts r and i denote real and imaginary, respectively. The parameters used are $k_yL = 10.0$, $\tilde{\nu} = \nu_{in}/(V_o/L) = 100.0$, and $\theta = 70^o$ where E_x is given by Eq. (38). The eigenfrequency is $\tilde{\omega}_r = 0.5307$ and $\tilde{\gamma} = 0.0716$. (a) Q vs. x/L. (b) $\tilde{\phi}$ vs. x/L.

A longer wavelength mode is now considered. We choose $k_yL = 0.1$ so that $k_yL \ll 1$, but still consider $\tilde{\nu} = 100.0$ as in the short wavelength case. Figure 11 is a plot of the density profile $n(x)/n_0$ and electric field profile $E_x(x)/E_{0x}$ for the same parameters as in Fig. 8. However, the range of x/L is expanded for comparison to the broadened mode structure. Figure 12 is a plot of Q (Fig. 12a) and $\tilde{\phi}$ (Fig. 12b) for the case of no electric field inhomogeneity ($\theta = 0^o$ or $E_x(x) = 0$). The eigenfrequency is $\tilde{\omega}_r = 0.0$ and $\tilde{\gamma} = 0.0930$. The character of Q is considerably different from the short wavelength case (Fig. 9a). The position of the minimum of the potential well is shifted to $x/L = 0.0$. Moreover, a "potential anti-well" exists for $-5.0 < x/L < 0.0$ which tends to inhibit mode penetration in this region. The corresponding eigenfunction $\tilde{\phi}$ (Fig. 12b) is also substantially different from the short wavelength case (Fig. 9b). First, the wave function has a surface wave character in that $\tilde{\phi} = \tilde{\phi}_0 \exp(-\kappa x)$. Second, the wavefunction is asymmetrical about the position of minimum Q_r, $x/L = 0.0$. The wavefunction falls off very rapidly in the region $-4.0 < x/L < 0.0$ which is due to the "potential anti-well" of Q in this region. For $x/L < -4.0$, $\tilde{\phi}$ falls off more gradually, similar to its behavior for $x/L > 10.0$. And finally, the wave function is very broad, extending out to $x/L = 50.0$.

Figure 13 is a plot of Q (Fig. 13a) and $\tilde{\phi}$ (Fig. 13b) versus x/L for the same parameters as Fig. 10, but now we take $\theta = 70^o$ so that the electric field is inhomogeneous (see Fig. 11). The eigenfrequency is $\tilde{\omega}_r = 0.0057$ and $\tilde{\gamma} = 0.0314$. Although both the wave potential Q and the wave eigenfunction $\tilde{\phi}$ now have imaginary components, Q and $\tilde{\phi}$ are quite similar to the no shear case. The wave function is centered about $x/L = 0.0$, has an asymmetrical nature, and extends up to $x/L = 50.0$. Thus, the

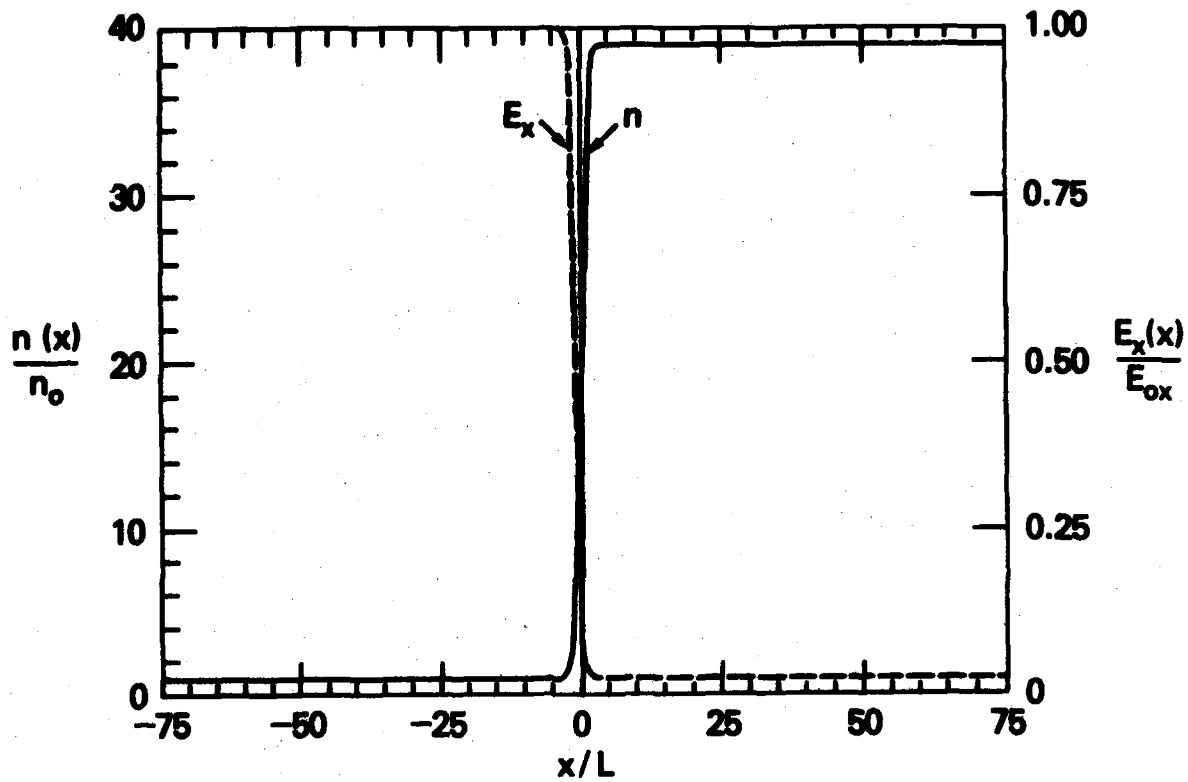

Fig. 11 Equilibrium density (Eq. (32) and electric field (Eq. (38)) profiles for $\varepsilon = 0.95$.

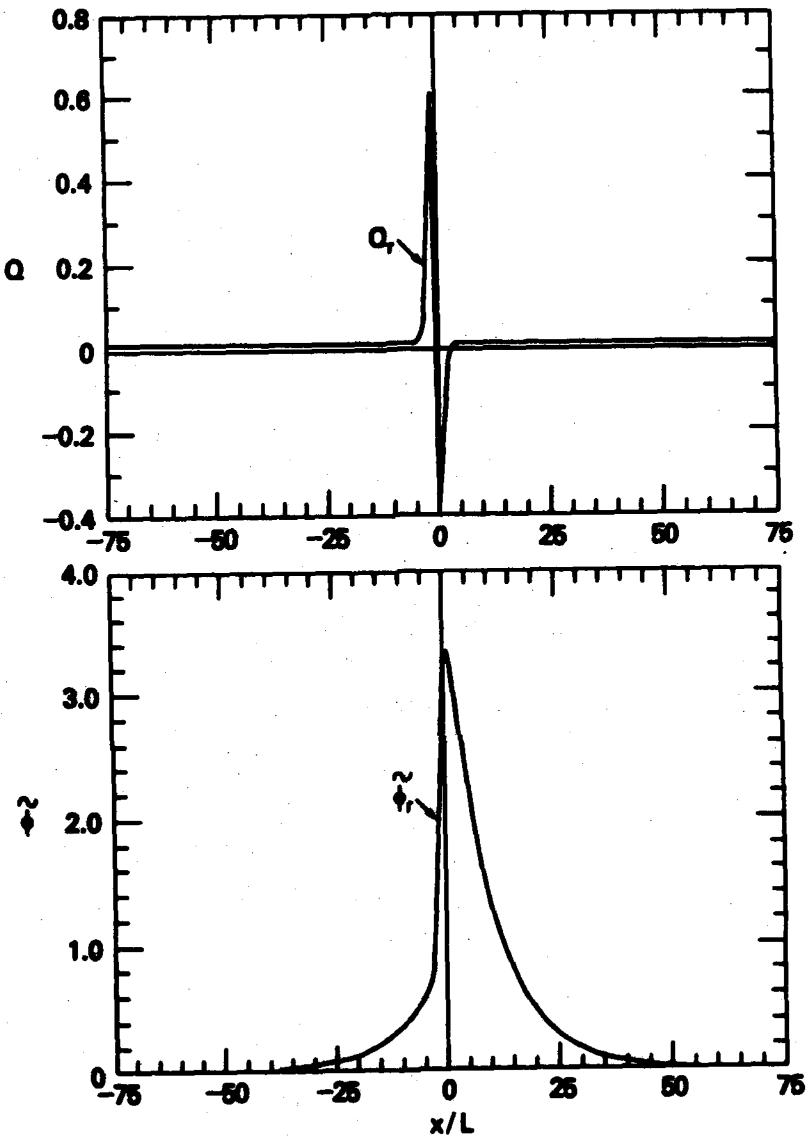

Fig. 12 Wave potential Q and wave eigenfunction $\tilde{\phi}$ as a function of x/L. The subscripts r and i denote real and imaginary, respectively. The parameters considered are $k_yL = 0.1$, $\tilde{\nu} = \nu_{in}/(V_o/L) = 100.0$, and $\theta = 0^{\circ}$ (i.e., $E_x = 0$). The eigenfrequency is $\tilde{\omega}_r = 0.0$ and $\tilde{\gamma} = 0.0930$. (a) Q vs. x/L. (b) $\tilde{\phi}$ vs. x/L.

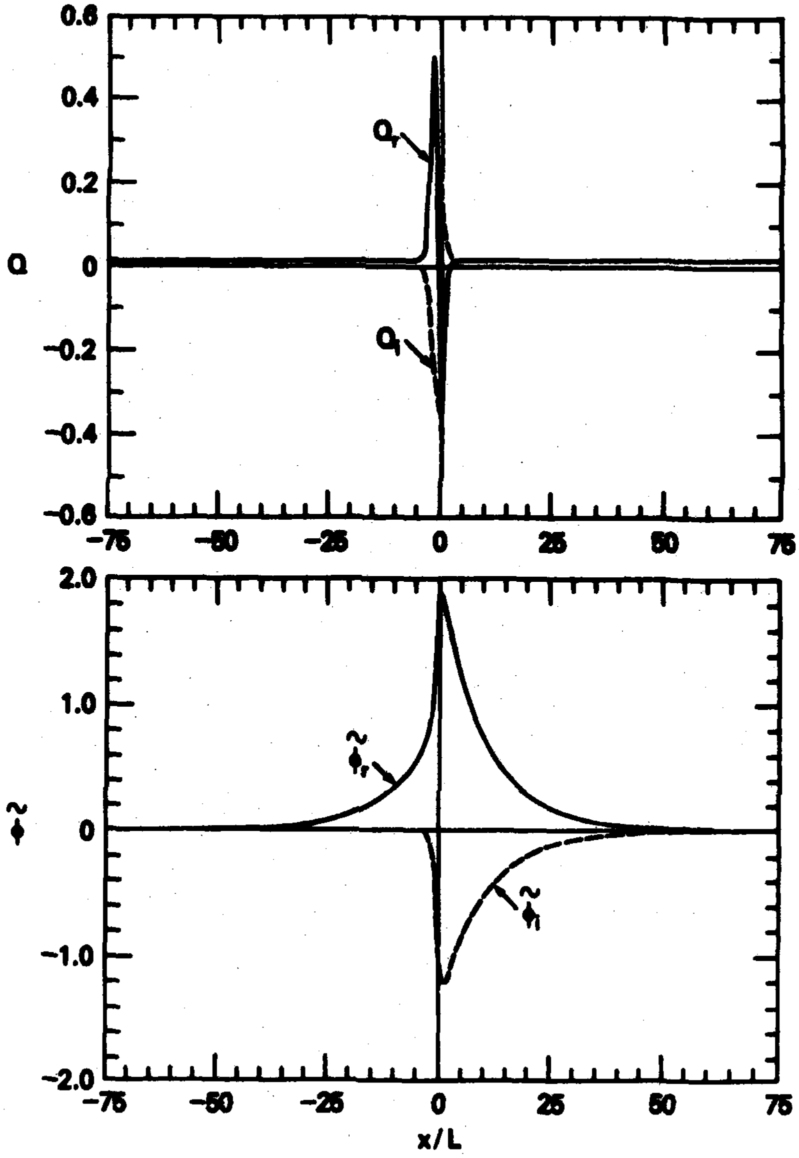

Fig. 13 Wave potential Q and wave eigenfunction $\tilde{\phi}$ as a function of x/L. The subscripts r and i denote real and imaginary, respectively. The parameters considered are $k_yL = 0.1$, $\tilde{\nu} = \nu_{in}/(V_o/L) = 100.0$, and $\theta = 70^o$ where E_x is given by Eq. (38). The eigenfrequency is $\tilde{\omega}_r = 0.0057$ and $\tilde{\gamma} = 0.0314$. (a) Q vs. x/L. (b) $\tilde{\phi}$ vs. x/L.

influence of the electric field inhomogeneity on the wave structure in the long wavelength regime ($k_yL \ll 1$) is much less pronounced than that in the short wavelength regime ($k_yL \gg 1$). However, the electric field inhomogeneity does reduce the growth rate of the mode significantly.

Finally we present Fig. 14 which is a marginal stability curve (i.e., $\gamma = 0$) of θ vs. k_yL where we have taken $\tilde{\nu} = 1.0$ (dashed curve) and and 100.0 (solid curve). Modes are stable ($\gamma < 0$) and unstable ($\gamma > 0$) above and below each of the curves, respectively. The ratio $E_x(x_o)/E_y$ is for the case $\tilde{\nu} = 100.0$ and has the following meaning. It is the ratio of E_x to E_y evaluated at $x = x_o$, where x_o is the position of mode localization. The position of mode localization is defined as the portion of the minimum value of Q_r, which corresponds to the maximum value of ϕ. For the parameters chosen, it is found that $x_o = 0$. The marginal stability criterion is then given by

$$\frac{E_x(x_o)}{E_y} > 0.05 \tan \theta_{ms} \tag{40}$$

where θ_{ms} is the value of θ at marginal stability and we have used Eqs. (32) and (38) with $\varepsilon = 0.95$. From Fig. 14 we find that

$$\theta_{ms} = 88 - 1.4\, k_yL \tag{41}$$

where θ_{ms} is measured in degrees. Substituting Eq. (41) into Eq. (40), we obtain

$$\frac{E_x(x_o)}{E_y} > \frac{0.05}{\tan(1.4k_yL)} \tag{42}$$

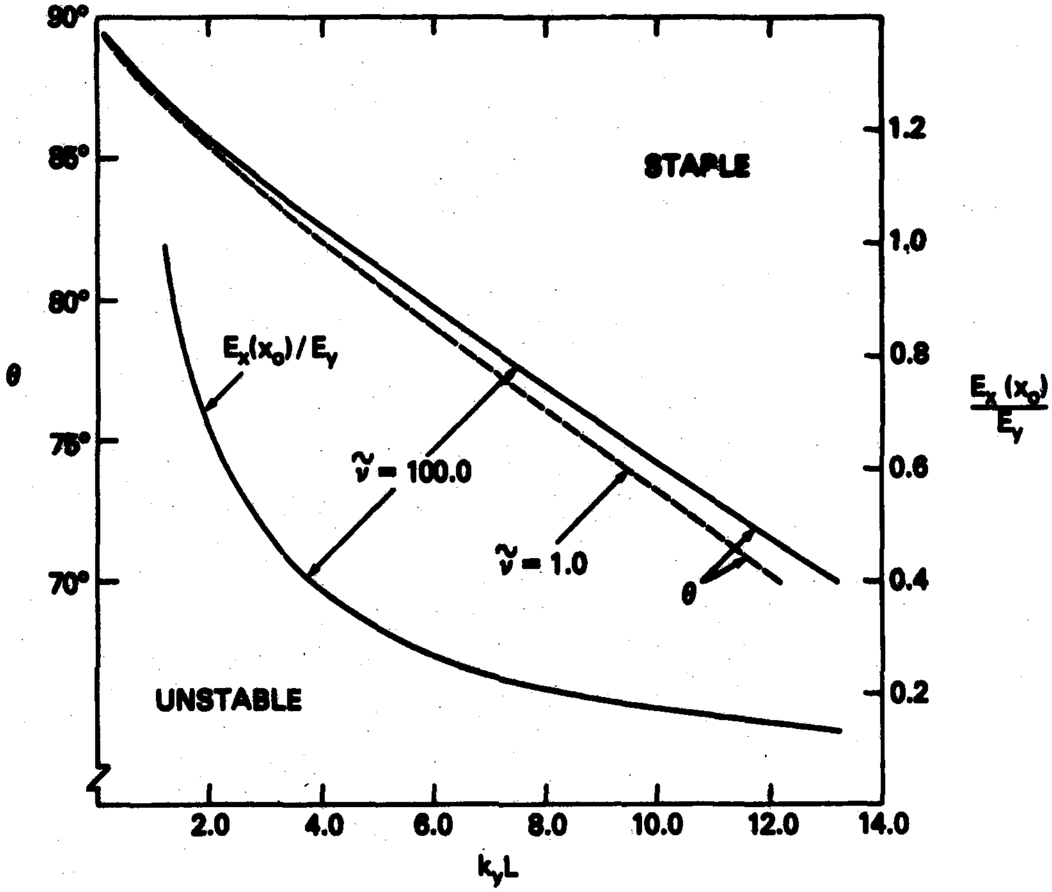

Fig. 14 Marginal stability curve of θ vs. k_yL for $\tilde{\nu} = 1.0$ (dashed curve) and $\tilde{\nu} = 100.0$ (solid curve). The mode is stable ($\gamma < 0$) and unstable ($\gamma > 0$) above and below each of these curves, respectively. The ratio $E_x(x_o)/E_y$ vs. k_yL is for the case $\tilde{\nu} = 100.0$ where $x_o/L = 0.0$ is the position of mode localization. In all of these curves, Eq. (38) has been used for $E_x(x)$.

or

$$\frac{E_x(x_o)}{E_y} > \frac{2.05}{k_y L} \tag{43}$$

for $k_y L \ll 36.0$. Note that Eq. (43) is qualitatively consistent with the result of Perkins and Doles (1975) in that there is an inverse relationship between $E_x(x_o)/E_y$ and k_y. Also, Eq. (43) is also quantitatively consistent (see Eq. (24)) since $D > L$ for the profiles used. Finally, as θ approaches 90^o, i.e., $E_y \to 0$, the wavenumber of the last unstable mode approaches 0. There is no instability at $\theta = 90^o$; this has been demonstrated analytically by Perkins et al. (1973).

IV. DISCUSSION

We have presented a general theory of the $\underset{\sim}{E} \times \underset{\sim}{B}$ instability allowing for an arbitrary (1) density profile, (2) inhomogeneous electric field parallel to the density gradient, and (3) ratio of the collision frequency to the eigenfrequency (i.e., ν_{in}/ω). A differential equation is derived which describes the structure of the mode in the direction of the inhomogeneity, which we have considered to be the x direction. The theory is restricted to wave numbers such that $k_y L \ll \Omega_i/\nu_{in}$ and $k_y L \ll \Omega_i/\omega$; since it has also been assumed that $\nu_{in}/\Omega_i \ll 1$ and $\omega/\Omega_i \ll 1$ this restriction is not important. This work is basically an extension of the analysis of Perkins and Doles (1975), whose theory is restricted to the regime $\nu_{in}/\omega \gg 1$ and $k_y L \gg 1$, and considers a specific density and electric field profile. The principal results of this study are as follows.

1. For a constant electric field profile, instability persists even when $E_y = 0$ ($\theta = 90^o$). In fact, instability also occurs for $E_y < 0$ ($\theta > 90^o$) when $\partial n/\partial x > 0$; this is contrary to the simple one dimensional result (i.e., $\underset{\sim}{k} = k_y \hat{e}_y$) which requires $E_y \partial n/\partial x > 0$ for instability. Thus, two-dimensional mode structure (i.e., $\underset{\sim}{k} = k_x \hat{e}_x + k_y \hat{e}_y$) is crucial to the instability (Eq. (18)) (Linson and Workman, 1971).

2. For an inhomogeneous electric field, an inhomogeneous $\underset{\sim}{E} \times \underset{\sim}{B}$ velocity occurs ($V_y(x) = - cE_x(x)/B$) which has a stabilizing influence on the mode. Moreover, the short wavelength modes ($k_y L \gg 1$) are preferentially stabilized over long wavelength modes ($k_y L \lesssim 1$). This result is consistent with the work of Perkins and Doles (1975).

a. The functional form of $E_x(x)$ is not critical to stabilization of the mode. In the absence of any plasma sources or sinks, the ion continuity equation gives the equilbrium relationship between the density (n(x)) and the electric field $E_x(x)$, as given by Eq. (7) (also, see Fig. 8). Perkins and Doles (1975) use this relationship in their analysis. However, we have considered other electric field profiles (e.g., $E_x(x) \propto n(x)$ and $E_x(x) \propto \tanh(x)/n(x)$). We have found that the instability is still stabilized by the velocity inhomogeneity, again preferentially stabilizing the shorter wavelength modes, but that the marginal stability curves are different from Fig. (13).

b. The mode is stabilized because of the x-dependent resonance $\omega - k_y V_{ey}(x)$ in Eq. (15). Terms proportional to $\partial V_{ey}/\partial x$ and $\partial^2 V_{ey}/\partial x^2$ are not important for stabilization.

c. Perkins et al. (1973) have shown analytically that the mode is stable for $E_y = 0$ and E_x given by Eq. (21). The numerical results presented here are consistent with this conclusion. However, we add that as $E_y \rightarrow 0$ then $k_y L \rightarrow 0$. This is clear from Fig. (14) by noting that $k_y L \rightarrow 0$ as $\theta \rightarrow 90^o$.

d. In general, it is found that as ν_{in} decreases the growth rate of the mode decreases; this is expected from linear theory (Eqs. (19) and (20)). However, in the case of an inhomogeneous electric field, the difference in growth rates between the strong and weak collisional limits considered is not significant (see Fig. (4)). Furthermore, the stabilization criterion is not sensitive to ν_{in} (see Fig. (14)).

These results are applicable to the development of the $\underset{\sim}{E} \times \underset{\sim}{B}$ instability in both barium releases and the high latitude F region ionosphere. First, the important aspects of an inhomogeneous electric field on barium cloud striations has been adequately addressed by Perkins and Doles (1975). In particular, they note that (1) the back side of a plasma cloud must steepen sufficiently so that it is almost one-dimensional to allow the mode to grow (i.e., $\underset{\sim}{E} \approx E_y \hat{e}_y$) and (2) the stabilization of the mode due to $E_x(x)$ may explain why the sides of a plasma cloud do not become unstable. Furthermore, from our studies, we might hypothesize that the "freezing" phenomenon in plasma cloud striations (see McDonald et al., 1981) could be due to shear stabilization effects, since shear stabilization acts preferentially on short wavelength modes, i.e., $k_y L \gg 1$, but not on long wavelength modes, i.e., $k_y L < 1$. Second, the role of an inhomogeneous electric field in the $\underset{\sim}{E} \times \underset{\sim}{B}$ instability can be very important in the structuring of plasma "blobs" observed in the high latitude F region. Experimental observations (Vickrey et al., 1980; Tsunoda and Vickrey, 1982) indicate structuring in both the east-west and north-south directions. Moreover, small-scale structuring of the walls of the "blobs" have also been observed and is attributed to the $\underset{\sim}{E} \times \underset{\sim}{B}$ instability and/or the current convective instability. The plasma configuration is not well-known but the morphology of the "blobs" appears to be very complex. Not only are there inhomogeneities anticipated in the electric field, but there are also neutral wind effects, field-aligned plasma currents, and possible coupling effects between the E and F regions. A complete theoretical treatment incorporating these effects is beyond the scope of this paper. However, the results of this analysis strongly suggest that in order for the $\underset{\sim}{E} \times \underset{\sim}{B}$ drift instability to be a viable candidate for structuring in the high latitude F region, then the ambient electric field must be orthogonal or nearly orthogonal to the density gradient. A more complete discussion of this problem will be deferred to a later report in which the influences of a field-aligned current and neutral wind are incorporated into this analysis.

ACKNOWLEDGMENTS

This work has been supported by the Defense Nuclear Agency and the Office of Naval Research.

REFERENCES

Chaturvedi, P.K. and S.L. Ossakow, "Nonlinear Stabilization of the E x B Gradient Drift Instability in Ionospheric Plasma Clouds," J. Geophys. Res., 84, 419, 1979.

Hoh, F.C., "Instability of Penning-Type Discharges," Phys. Fluids, 6, 1184, 1963.

Keskinen, M.J. and S.L. Ossakow, "Effect of Different Initial Conditions on the Evolution of the E x B Gradient Drift Instability in Ionospheric Plasma Clouds," NRL Memo Report 4490, April 1981.

Linson, L.M. and J.B. Workman, "Formation of Striations in Ionospheric Plasma Clouds," J. Geophys. Res., 75, 3211, 1970.

McDonald, B.E., S.L. Ossakow, S.T. Zalesak, and N.J. Zabusky, "Scale Sizes and Lifetimes of F Region Plasma Cloud Striations as Determined by the Condition of Marginal Stability," J. Geophys. Res., 86, 5775, 1981.

Ossakow, S.L., P.K. Chaturvedi, and J.B. Workman, "High Altitude Limit of the Gradient Drift Instability," J. Geophys. Res., 83, 2691, 1978.

Ossakow, S.L., "Ionospheric Irregularities," Rev. Geophys. Space Phys., 17, 521, 1979.

Ossakow, S.L., M.J. Keskinen, and S.T. Zalesak, "Ionospheric Irregularity Physics Modelling," AIAA 20th Aerospace Sciences Meeting, AIAA-82-0147, 1982.

Perkins, F.W., N.J. Zabusky, and J.H. Doles III, "Deformation and Striation of Plasma Clouds in the Ionosphere, 1," J. Geophys. Res., 78, 697, 1973.

Perkins, F.W. and J.H. Doles III, "Velocity Shear and the E x B Instability," J. Geophys. Res., 80, 211, 1975.

Scannapieco, A.J., S.L. Ossakow, S.R. Goldman, and J.M. Pierre, "Plasma Cloud Late Time Striation Spectra," J. Geophys. Res., 81, 6037, 1976.

Shiau, J.N. and A. Simon, "Onset of Striations in Barium Clouds," Phys. Rev. Lett., 29, 1664, 1972.

Simon, A., "Instability of a Partially Ionized Plasma in Crossed Electric and Magnetic Fields," Phys. Fluids, 6, 382, 1963.

Simon, A., "Growth and Stability of Artificial Ion Clouds in the Ionosphere," J. Geophys. Res., 75, 6287, 1970.

Tsunoda, R.T. and J.F. Vickrey, "Evidence of East-West Structure in Large-Scale F-Region Plasma Enhancements in the Auroral Zone," submitted to J. Geophys. Res., 1982.

Vickrey, J.F., C.L. Rino, and T.A. Potemra, "Chatanika/Triad Observations of Unstable Ionization Enhancements in the Auroral F-Region," Geophys. Res. Lett., 7, 789, 1980.

Völk, H.J., and G. Haerendel, "Striations in Ionospheric Ion Clouds, 1," J. Geophys. Res., 76, 4541, 1971.

Zabusky, N.J., J.H. Doles III, and F.W. Perkins, "Deformation and Striation of Plasma Clouds in the Ionosphere, 2. Numerical Simulation of a Nonlinear Two-Dimensional Model," J. Geophys. Res., 78, 711, 1973.

DISTRIBUTION LIST

DEPARTMENT OF DEFENSE

ASSISTANT SECRETARY OF DEFENSE
COMM, CMD, CONT 7 INTELL
WASHINGTON, D.C. 20301
 01CY ATTN J. BABCOCK
 01CY ATN M. EPSTEIN

DIRECTOR
COMMAND CONTROL TECHNICAL CENTER
PENTAGON RM BE 685
WASHINGTON, D.C. 20301
 01CY ATTN C-650
 01CY ATTN C-312 R. MASON

DIRECTOR
DEFENSE ADVANCED RSCH PROJ AGENCY
ARCHITECT BUILDING
1400 WILSON BLVD.
ARLINGTON, VA. 22209
 01CY ATTN NUCLEAR MONITORING RESEARCH
 01CY ATTN STRATEGIC TECH OFFICE

DEFENSE COMMUNICATION ENGINEER CENTER
1860 WIEHLE AVENUE
RESTON, VA. 22090
 01CY ATTN CODE R410
 01CY ATTN CODE R812

DIRECTOR
DEFENSE COMMUNICATIONS AGENCY
WASHINGTON, D.C. 20305
 (ADR CNWDI: ATTN CODE 240 FOR)
 01CY ATTN CODE 101B

DEFENSE TECHNICAL INFORMATION CENTER
CAMERON STATION
ALEXANDRIA, VA. 22314
 02CY

DIRECTOR
DEFENSE NUCLEAR AGENCY
WASHINGTON, D.C. 20305
 01CY ATTN STVL
 04CY ATTN TITL
 01CY ATTN DDST
 03CY ATTN RAAE

COMMANDER
FIELD COMMAND
DEFENSE NUCLEAR AGENCY
KIRTLAND, AFB, NM 87115
 01CY ATTN FCPR

DIRECTOR
INTERSERVICE NUCLEAR WEAPONS SCHOOL
KIRTLAND AFB, NM 87115
 01CY ATTN DOCUMENT CONTROL

JOINT CHIEFS OF STAFF
WASHINGTON, D.C. 20301
 01CY ATTN J-3 WWMCCS EVALUATION OFFICE

DIRECTOR
JOINT STRAT TGT PLANNING STAFF
OFFUTT AFB
OMAHA, NB 68113
 01CY ATTN JLTW-2
 01CY ATTN JPST G. GOETZ

CHIEF
LIVERMORE DIVISION FLD COMMAND DNA
DEPARTMENT OF DEFENSE
LAWRENCE LIVERMORE LABORATORY
P.O. BOX 808
LIVERMORE, CA 94550
 01CY ATTN FCPRL

COMMANDANT
NATO SCHOOL (SHAPE)
APO NEW YORK 09172
 01CY ATTN U.S. DOCUMENTS OFFICER

UNDER SECY OF DEF FOR RSCH & ENGRG
DEPARTMENT OF DEFENSE
WASHINGTON, D.C. 20301
 01CY ATTN STRATEGIC & SPACE SYSTEMS (OS)

WWMCCS SYSTEM ENGINEERING ORG
WASHINGTON, D.C. 20305
 01CY ATTN R. CRAWFORD

COMMANDER/DIRECTOR
ATMOSPHERIC SCIENCES LABORATORY
U.S. ARMY ELECTRONICS COMMAND
WHITE SANDS MISSILE RANGE, NM 88002
 01CY ATTN DELAS-EO F. NILES

DIRECTOR
BMD ADVANCED TECH CTR
HUNTSVILLE OFFICE
P.O. BOX 1500
HUNTSVILLE, AL 35807
  01CY ATTN ATC-T MELVIN T. CAPPS
  01CY ATTN ATC-O W. DAVIES
  01CY ATTN ATC-R DON RUSS

PROGRAM MANAGER
BMD PROGRAM OFFICE
5001 EISENHOWER AVENUE
ALEXANDRIA, VA 22333
  01CY ATTN DACS-BMT J. SHEA

CHIEF C-E- SERVICES DIVISION
U.S. ARMY COMMUNICATIONS CMD
PENTAGON RM IB269
WASHINGTON, D.C. 20310
  01CY ATTN C- E-SERVICES DIVISION

COMMANDER
FRADCOM TECHNICAL SUPPORT ACTIVITY
DEPARTMENT OF THE ARMY
FORT MONMOUTH, N.J. 07703
  01CY ATTN DRSEL-NL-RD H. BENNET
  01CY ATTN DRSEL-PL-ENV H. BOMKE
  01CY ATTN J.E. QUIGLEY

COMMANDER
HARRY DIAMOND LABORATORIES
DEPARTMENT OF THE ARMY
2800 POWDER MILL ROAD
ADELPHI, MD 20783
    (CNWDI-INNER ENVELOPE: ATTN: DELHD-RBH)
  01CY ATTN DELHD-TI M. WEINER
  01CY ATTN DELHD-RB R. WILLIAMS
  01CY ATTN DELHD-NP F. WIMENITZ
  01CY ATTN DELHD-NP C. MOAZED

COMMANDER
U.S. ARMY COMM-ELEC ENGRG INSTAL AGY
FT. HUACHUCA, AZ 85613
  01CY ATTN CCC-EMEO GEORGE LANE

COMMANDER
U.S. ARMY FOREIGN SCIENCE & TECH CTR
220 7TH STREET, NE
CHARLOTTESVILLE, VA 22901
  01CY ATTN DRXST-SD
  01CY ATTN R. JONES

COMMANDER
U.S. ARMY MATERIAL DEV & READINESS CMD
5001 EISENHOWER AVENUE
ALEXANDRIA, VA 22333
  01CY ATTN DRCLDC J.A. BENDER

COMMANDER
U.S. ARMY NUCLEAR AND CHEMICAL AGENCY
7500 BACKLICK ROAD
BLDG 2073
SPRINGFIELD, VA 22150
  01CY ATTN LIBRARY

DIRECTOR
U.S. ARMY BALLISTIC RESEARCH LABORATORY
ABERDEEN PROVING GROUND, MD 21005
  01CY ATTN TECH LIBRARY EDWARD BAICY

COMMANDER
U.S. ARMY SATCOM AGENCY
FT. MONMOUTH, NJ 07703
  01CY ATTN DOCUMENT CONTROL

COMMANDER
U.S. ARMY MISSILE INTELLIGENCE AGENCY
REDSTONE ARSENAL, AL 35809
  01CY ATTN JIM GAMBLE

DIRECTOR
U.S. ARMY TRADOC SYSTEMS ANALYSIS ACTIVITY
WHITE SANDS MISSILE RANGE, NM 88002
  01CY ATTN ATAA-SA
  01CY ATTN TCC/F. PAYAN JR.
  01CY ATTN ATTA-TAC LTC J. HESSE

COMMANDER
NAVAL ELECTRONIC SYSTEMS COMMAND
WASHINGTON, D.C. 20360
  01CY ATTN NAVALEX 034 T. HUGHES
  01CY ATTN PME 117
  01CY ATTN PME 117-T
  01CY ATTN CODE 5011

COMMANDING OFFICER
NAVAL INTELLIGENCE SUPPORT CTR
4301 SUITLAND ROAD, BLDG. 5
WASHINGTON, D.C. 20390
  01CY ATTN MR. DUBBIN STIC 12
  01CY ATTN NISC-50
  01CY ATTN CODE 5404 J. GALET

COMMANDER
NAVAL OCCEAN SYSTEMS CENTER
SAN DIEGO, CA 92152
  03CY ATTN CODE 532 W. MOLER
  01CY ATTN CODE 0230 C. BAGGETT
  01CY ATTN CODE 81 R. EASTMAN

DIRECTOR
NAVAL RESEARCH LABORATORY
WASHINGTON, D.C. 20375
 01CY ATTN CODE 4700 S. L. Ossakow
 26 CYS IF UNCLASS. 1 CY IF CLASS)
 01CY ATTN CODE 4701 JACK D. BROWN
 01CY ATTN CODE 4780 BRANCH HEAD (150
 CYS IF UNCLASS, 1 CY IF CLASS)
 01CY ATTN CODE 7500
 01CY ATTN CODE 7550
 01CY ATTN CODE 7580
 01CY ATTN CODE 7551
 01CY ATTN CODE 7555
 01CY ATTN CODE 4730 E. MCLEAN
 01CY ATTN CODE 4187

COMMANDER
NAVAL SEA SYSTEMS COMMAND
WASHINGTON, D.C. 20362
 01CY ATTN CAPT R. PITKIN

COMMANDER
NAVAL SPACE SURVEILLANCE SYSTEM
DAHLGREN, VA 22448
 01CY ATTN CAPT J.H. BURTON

OFFICER-IN-CHARGE
NAVAL SURFACE WEAPONS CENTER
WHITE OAK, SILVER SPRING, MD 20910
 01CY ATTN CODE F31

DIRECTOR
STRATEGIC SYSTEMS PROJECT OFFICE
DEPARTMENT OF THE NAVY
WASHINGTON, D.C. 20376
 01CY ATTN NSP-2141
 01CY ATTN NSSP-2722 FRED WIMBERLY

COMMANDER
NAVAL SURFACE WEAPONS CENTER
DAHLGREN LABORATORY
DAHLGREN, VA 22448
 01CY ATTN CODE DF-14 R. BUTLER

OFFICER OF NAVAL RESEARCH
ARLINGTON, VA 22217
 01CY ATTN CODE 465
 01CY ATTN CODE 461
 01CY ATTN CODE 402
 01CY ATTN CODE 420
 01CY ATTN CODE 421

COMMANDER
AEROSPACE DEFENSE COMMAND/DC
DEPARTMENT OF THE AIR FORCE
ENT AFB, CO 80912
 01CY ATTN DC MR. LONG

COMMANDER
AEROSPACE DEFENSE COMMAND/XPD
DEPARTMENT OF THE AIR FORCE
ENT AFB, CO 80912
 01CY ATTN XPDQQ
 01CY ATTN XP

AIR FORCE GEOPHYSICS LABORATORY
HANSCOM AFB, MA 01731
 01CY ATTN OPR HAROLD GARDNER
 01CY ATTN LKB KENNETH S.W. CHAMPION
 01CY ATTN OPR ALVA T. STAIR
 01CY ATTN PHP JULES AARONS
 01CY ATTN PHD JURGEN BUCHAU
 01CY ATTN PHD JOHN P. MULLEN

AF WEAPONS LABORATORY
KIRTLAND AFT, NM 87117
 01CY ATTN SUL
 01CY ATTN CA ARTHUR H. GUENTHER
 01CY ATTN NTYCE 1LT. G. KRAJEI

AFTAC
PATRICK AFB, FL 32925
 01CY ATTN TF/MAJ WILEY
 01CY ATTN TN

AIR FORCE AVIONICS LABORATORY
WRIGHT-PATTERSON AFB, OH 45433
 01CY ATTN AAD WADE HUNT
 01CY ATTN AAD ALLEN JOHNSON

DEPUTY CHIEF OF STAFF
RESEARCH, DEVELOPMENT, & ACQ
DEPARTMENT OF THE AIR FORCE
WASHINGTON, D.C. 20330
 01CY ATTN AFRDQ

HEADQUATERS
ELECTRONIC SYSTEMS DIVISION/XR
DEPARTMENT OF THE AIR FORCE
HANSCOM AFB, MA 01731
 01CY ATTN XR J. DEAS

HEADQUATERS
ELECTRONIC SYSTEMS DIVISION/YSEA
DEPARTMENT OF THE AIR FORCE
HANSCOM AFB, MA 01732
 01CY ATTN YSEA

HEADQUATERS
ELECTRONIC SYSTEMS DIVISION/DC
DEPARTMENT OF THE AIR FORCE
HANSCOM AFB, MA 01731
 01CY ATTN DCKC MAJ J.C. CLARK

COMMANDER
FOREIGN TECHNOLOGY DIVISION, AFSC
WRIGHT-PATTERSON AFB, OH 45433
01CY ATTN NICD LIBRARY
01CY ATTN ETDP B. BALLARD

COMMANDER
ROME AIR DEVELOPMENT CENTER, AFSC
GRIFFISS AFB, NY 13441
01CY ATTN DOC LIBRARY/TSLD
01CY ATTN OCSE V. COYNE

SAMSO/SZ
POST OFFICE BOX 92960
WORLDWAY POSTAL CENTER
LOS ANGELES, CA 90009
(SPACE DEFENSE SYSTEMS)
01CY ATTN SZJ

STRATEGIC AIR COMMAND/XPFS
OFFUTT AFB, NB 68113
01CY ATTN XPFS MAJ B. STEPHAN
01CY ATTN ADWATE MAJ BRUCE BAUER
01CY ATTN NRT
01CY ATTN DOK CHIEF SCIENTIST

SAMSO/SK
P.O. BOX 92960
WORLDWAY POSTAL CENTER
LOS ANGELES, CA 90009
01CY ATTN SKA (SPACE COMM SYSTEMS)
M. CLAVIN

SAMSO/MN
NORTON AFB, CA 92409
(MINUTEMAN)
01CY ATTN MNNL LTC KENNEDY

COMMANDER
ROME AIR DEVELOPMENT CENTER, AFSC
HANSCOM AFB, MA 01731
01CY ATTN EEP A. LORENTZEN

DEPARTMENT OF ENERGY
LIBRARY ROOM G-042
WASHINGTON, D.C. 20545
01CY ATTN DOC CON FOR A. LABOWITZ

DEPARTMENT OF ENERGY
ALBUQUERQUE OPERATIONS OFFICE
P.O. BOX 5400
ALBUQUERQUE, NM 87115
01CY ATTN DOC CON FOR D. SHERWOOD

EG&G, INC.
LOS ALAMOS DIVISION
P.O. BOX 809
LOS ALAMOS, NM 85544
01CY ATTN DOC CON FOR J. BREEDLOVE

UNIVERSITY OF CALIFORNIA
LAWRENCE LIVERMORE LABORATORY
P.O. BOX 808
LIVERMORE, CA 94550
01CY ATTN DOC CON FOR TECH INFO DEPT
01CY ATTN DOC CON FOR L-389 R. OTT
01CY ATTN DOC CON FOR L-31 R. HAGER
01CY ATTN DOC CON FOR L-46 F. SEWARD

LOS ALAMOS NATIONAL LABORATORY
P.O. BOX 1663
LOS ALAMOS, NM 87545
01CY ATTN DOC CON FOR J. WOLCOTT
01CY ATTN DOC CON FOR R.F. TASCHEK
01CY ATTN DOC CON FOR E. JONES
01CY ATTN DOC CON FOR J. MALIK
01CY ATTN DOC CON FOR R. JEFFRIES
01CY ATTN DOC CON FOR J. ZINN
01CY ATTN DOC CON FOR P. KEATON
01CY ATTN DOC CON FOR D. WESTERVELT

SANDIA LABORATORIES
P.O. BOX 5800
ALBUQUERQUE, NM 87115
01CY ATTN DOC CON FOR W. BROWN
01CY ATTN DOC CON FOR A. THORNBROUGH
01CY ATTN DOC CON FOR T. WRIGHT
01CY ATTN DOC CON FOR D. DAHLGREN
01CY ATTN DOC CON FOR 3141
01CY ATTN DOC CON FOR SPACE PROJECT DIV

SANDIA LABORATORIES
LIVERMORE LABORATORY
P.O. BOX 969
LIVERMORE, CA 94550
01CY ATTN DOC CON FOR B. MURPHEY
01CY ATTN DOC CON FOR T. COOK

OFFICE OF MILITARY APPLICATION
DEPARTMENT OF ENERGY
WASHINGTON, D.C. 20545
01CY ATTN DOC CON DR. YO SONG

OTHER GOVERNMENT

DEPARTMENT OF COMMERCE
NATIONAL BUREAU OF STANDARDS
WASHINGTON, D.C. 20234
(ALL CORRES: ATTN SEC OFFICER FOR)
01CY ATTN R. MOORE

INSTITUTE FOR TELECOM SCIENCES
NATIONAL TELECOMMUNICATIONS & INFO ADMIN
BOULDER, CO 80303
 01CY ATTN A. JEAN (UNCLASS ONLY)
 01CY ATTN W. UTLAUT
 01CY ATTN D. CROMBIE
 01CY ATTN L. BERRY

NATIONAL OCEANIC & ATMOSPHERIC ADMIN
ENVIRONMENTAL RESEARCH LABORATORIES
DEPARTMENT OF COMMERCE
BOULDER, CO 80302
 01CY ATTN R. GRUBB
 01CY ATTN AERONOMY LAB G. REID

DEPARTMENT OF DEFENSE CONTRACTORS

AEROSPACE CORPORATION
P.O. BOX 92957
LOS ANGELES, CA 90009
 01CY ATTN I. GARFUNKEL
 01CY ATTN T. SALMI
 01CY ATTN V. JOSEPHSON
 01CY ATTN S. BOWER
 01CY ATTN N. STOCKWELL
 01CY ATTN D. OLSEN

ANALYTICAL SYSTEMS ENGINEERING CORP
5 OLD CONCORD ROAD
BURLINGTON, MA 01803
 01CY ATTN RADIO SCIENCES

BERKELEY RESEARCH ASSOCIATES, INC.
P.O. BOX 983
BERKELEY, CA 94701
 01CY ATTN J. WORKMAN
 01CY ATTN C. PRETTIE

BOEING COMPANY, THE
P.O. BOX 3707
SEATTLE, WA 98124
 01CY ATTN G. KEISTER
 01CY ATTN D. MURRAY
 01CY ATTN G. HALL
 01CY ATTN J. KENNEY

BROWN ENGINEERING COMPANY, INC.
CUMMINGS RESEARCH PARK
HUNTSVILLE, AL 35807
 01CY ATTN ROMEO A. DELIBERIS

CALIFORNIA AT SAN DIEGO, UNIV OF
P.O. BOX 6049
SAN DIEGO, CA 92106

CHARLES STARK DRAPER LABORATORY, INC.
555 TECHNOLOGY SQUARE
CAMBRIDGE, MA 02139
 01CY ATTN D.B. COX
 01CY ATTN J.P. GILMORE

COMSAT LABORATORIES
LINTHICUM ROAD
CLARKSBURG, MD 20734
 01CY ATTN G. HYDE

CORNELL UNIVERSITY
DEPARTMENT OF ELECTRICAL ENGINEERING
ITHACA, NY 14850
 01CY ATTN D.T. FARLEY, JR.

ELECTROSPACE SYSTEMS, INC.
BOX 1359
RICHARDSON, TX 75080
 01CY ATTN H. LOGSTON
 01CY ATTN SECURITY (PAUL PHILLIPS)

ESL, INC.
495 JAVA DRIVE
SUNNYVALE, CA 94086
 01CY ATTN J. ROBERTS
 01CY ATTN JAMES MARSHALL

GENERAL ELECTRIC COMPANY
SPACE DIVISION
VALLEY FORGE SPACE CENTER
GODDARD BLVD KING OF PRUSSIA
P.O. BOX 8555
PHILADELPHIA, PA 19101
 01CY ATTN M.H. BORTNER SPACE SCI LAB

GENERAL ELECTRIC COMPANY
P.O. BOX 1122
SYRACUSE, NY 13201
 01CY ATTN F. REIBERT

GENERAL ELECTRIC TECH SERVICES CO., INC.
HMES
COURT STREET
SYRACUSE, NY 13201
 01CY ATTN G. MILLMAN

GENERAL RESEARCH CORPORATION
SANTA BARBARA DIVISION
P.O. BOX 6770
SANTA BARBARA, CA 93111
 01CY ATTN JOHN ISE, JR.
 01CY ATTN JOEL GARBARINO

GEOPHYSICAL INSTITUTE
UNIVERSITY OF ALASKA
FAIRBANKS, AK 99701
(ALL CLASS ATTN: SECURITY OFFICER)
01CY ATTN T.N. DAVIS (UNCLASS ONLY)
01CY ATTN TECHNICAL LIBRARY
01CY ATTN NEAL BROWN (UNCLASS ONLY)

GTE SYLVANIA, INC.
ELECTRONICS SYSTEMS GRP-EASTERN DIV
77 A STREET
NEEDHAM, MA 02194
01CY ATTN MARSHALL CROSS

HSS, INC.
2 ALFRED CIRCLE
BEDFORD, MA 01730
01CY ATTN DONALD HANSEN

ILLINOIS, UNIVERSITY OF
107 COBLE HALL
150 DAVENPORT HOUSE
CHAMPAIGN, IL 61820
(ALL CORRES ATTN DAN MCCLELLAND)
01CY ATTN K. YEH

INSTITUTE FOR DEFENSE ANALYSES
400 ARMY-NAVY DRIVE
ARLINGTON, VA 22202
01CY ATTN J.M. AEIN
01CY ATTN ERNEST BAUER
01CY ATTN HANS WOLFARD
01CY ATTN JOEL BENGSTON

INTL TEL & TELEGRAPH CORPORATION
500 WASHINGTON AVENUE
NUTLEY, NJ 07110
01CY ATTN TECHNICAL LIBRARY

JAYCOR
11011 TORREYANA ROAD
P.O. BOX 85154
SAN DIEGO, CA 92138
01CY ATTN J.L. SPERLING

JOHNS HOPKINS UNIVERSITY
APPLIED PHYSICS LABORATORY
JOHNS HOPKINS ROAD
LAUREL, MD 20707
01CY ATTN DOCUMENT LIBRARIAN
01CY ATTN THOMAS POTEMRA
01CY ATTN JOHN DASSOULAS
01CY ATTN DR. DONALD J. WILLIAMS

KAMAN SCIENCES CORP
P.O. BOX 7463
COLORADO SPRINGS, CO 80933
01CY ATTN T. MEAGHER

KAMAN TEMPO-CENTER FOR ADVANCED STUDIES
816 STATE STREET (P.O DRAWER QQ)
SANTA BARBARA, CA 93102
01CY ATTN DASIAC
01CY ATTN TIM STEPHANS
01CY ATTN WARREN S. KNAPP
01CY ATTN WILLIAM MCNAMARA
01CY ATTN B. GAMBILL

LINKABIT CORP
10453 ROSELLE
SAN DIEGO, CA 92121
01CY ATTN IRWIN JACOBS

LOCKHEED MISSILES & SPACE CO., INC
P.O. BOX 504
SUNNYVALE, CA 94088
01CY ATTN DEPT 60-12
01CY ATTN D.R. CHURCHILL

LOCKHEED MISSILES & SPACE CO., INC.
3251 HANOVER STREET
PALO ALTO, CA 94304
01CY ATTN MARTIN WALT DEPT 52-12
01CY ATTN W.L. IMHOF DEPT 52-12
01CY ATTN RICHARD G. JOHNSON DEPT 52-12
01CY ATTN J.B. CLADIS DEPT 52-12

LOCKHEED MISSILE & SPACE CO., INC.
HUNTSVILLE RESEARCH & ENGR. CTR.
4800 BRADFORD DRIVE
HUNTSVILLE, AL 35807
ATTN DALE H. DIVIS

MARTIN MARIETTA CORP
ORLANDO DIVISION
P.O. BOX 5837
ORLANDO, FL 32805
01CY ATTN R. HEFFNER

M.I.T. LINCOLN LABORATORY
P.O. BOX 73
LEXINGTON, MA 02173
01CY ATTN DAVID M. TOWLE
01CY ATTN P. WALDRON
01CY ATTN L. LOUGHLIN
01CY ATTN D. CLARK

MCDONNEL DOUGLAS CORPORATION
5301 BOLSA AVENUE
HUNTINGTON BEACH, CA 92647
01CY ATTN N. HARRIS
01CY ATTN J. MOULE
01CY ATTN GEORGE MROZ
01CY ATTN W. OLSON
01CY ATTN R.W. HALPRIN
01CY ATTN TECHNICAL LIBRARY SERVICES

MISSION RESEARCH CORPORATION
735 STATE STREET
SANTA BARBARA, CA 93101
01CY ATTN P. FISCHER
01CY ATTN W.F. CREVIER
01CY ATTN STEVEN L. GUTSCHE
01CY ATTN D. SAPPENFIELD
01CY ATTN R. BOGUSCH
01CY ATTN R. HENDRICK
01CY ATTN RALPH KILB
01CY ATTN DAVE SOWLE
01CY ATTN F. FAJEN
01CY ATTN M. SCHEIBE
01CY ATTN CONRAD L. LONGMIRE
01CY ATTN WARREN A. SCHLUETER

MITRE CORPORATION, THE
P.O. BOX 208
BEDFORD, MA 01730
01CY ATTN JOHN MORGANSTERN
01CY ATTN G. HARDING
01CY ATTN C.E. CALLAHAN

MITRE CORP
WESTGATE RESEARCH PARK
1820 DOLLY MADISON BLVD
MCLEAN, VA 22101
01CY ATTN W. HALL
01CY ATTN W. FOSTER

PACIFIC-SIERRA RESEARCH CORP
1456 CLOVERFIELD BLVD.
SANTA MONICA, CA 90404
01CY ATTN E.C. FIELD, JR.

PENNSYLVANIA STATE UNIVERSITY
IONOSPHERE RESEARCH LAB
318 ELECTRICAL ENGINEERING EAST
UNIVERSITY PARK, PA 16802
(NO CLASS TO THIS ADDRESS)
01CY ATTN IONOSPHERIC RESEARCH LAB

PHOTOMETRICS, INC.
442 MARRETT ROAD
LEXINGTON, MA 02173
01CY ATTN IRVING L. KOFSKY

PHYSICAL DYNAMICS, INC.
P.O. BOX 3027
BELLEVUE, WA 98009
01CY ATTN E.J. FREMOUW

PHYSICAL DYNAMICS, INC.
P.O. BOX 10367
OAKLAND, CA 94610
ATTN A. THOMSON

R & D ASSOCIATES
P.O. BOX 9695
MARINA DEL REY, CA 90291
01CY ATTN FORREST GILMORE
01CY ATTN BRYAN GABBARD
01CY ATTN WILLIAM B. WRIGHT, JR.
01CY ATTN ROBERT F. LELEVIER
01CY ATTN WILLIAM J. KARZAS
01CY ATTN H. ORY
01CY ATTN C. MACDONALD
01CY ATTN R. TURCO

RAND CORPORATION, THE
1700 MAIN STREET
SANTA MONICA, CA 90406
01CY ATTN CULLEN CRAIN
01CY ATTN ED BEDROZIAN

RAYTHEON CO.
528 BOSTON POST ROAD
SUDBURY, MA 01776
01CY ATTN BARBARA ADAMS

RIVERSIDE RESEARCH INSTITUTE
80 WEST END AVENUE
NEW YORK, NY 10023
01CY ATTN VINCE TRAPANI

SCIENCE APPLICATIONS, INC.
P.O. BOX 2351
LA JOLLA, CA 92038
01CY ATTN LEWIS M. LINSON
01CY ATTN DANIEL A. HAMLIN
01CY ATTN E. FRIEMAN
01CY ATTN E.A. STRAKER
01CY ATTN CURTIS A. SMITH
01CY ATTN JACK MCDOUGALL

SCIENCE APPLICATIONS, INC
1710 GOODRIDGE DR.
MCLEAN, VA 22102
ATTN: J. COCKAYNE

SRI INTERNATIONAL
333 RAVENSWOOD AVENUE
MENLO PARK, CA 94025
  01CY ATTN DONALD NEILSON
  01CY ATTN ALAN BURNS
  01CY ATTN G. SMITH
  01CY ATTN L.L. COBB
  01CY ATTN DAVID A. JOHNSON
  01CY ATTN WALTER G. CHESNUT
  01CY ATTN CHARLES L. RINO
  01CY ATTN WALTER JAYE
  01CY ATTN M. BARON
  01CY ATTN RAY L. LEADABRAND
  01CY ATTN G. CARPENTER
  01CY ATTN G. PRICE
  01CY ATTN J. PETERSON
  01CY ATTN R. HAKE, JR.
  01CY ATTN V. GONZALES
  01CY ATTN D. MCDANIEL

STEWART RADIANCE LABORATORY
UTAH STATE UNIVERSITY
1 DE ANGELO DRIVE
BEDFORD, MA 01730
  01CY ATTN J. ULWICK

TECHNOLOGY INTERNATIONAL CORP
75 WIGGINS AVENUE
BEDFORD, MA 01730
  01CY ATTN W.P. BOQUIST

TRW DEFENSE & SPACE SYS GROUP
ONE SPACE PARK
REDONDO BEACH, CA 90278
  01CY ATTN R. K. PLEBUCH
  01CY ATTN S. ALTSCHULER
  01CY ATTN D. DEE

VISIDYNE
SOUTH BEDFORD STREET
BURLINGTON, MASS 01803
  01CY ATTN W. REIDY
  01CY ATTN J. CARPENTER
  01CY ATTN C. HUMPHREY

IONOSPHERIC MODELING DISTRIBUTION LIST
(UNCLASSIFIED ONLY)

PLEASE DISTRIBUTE ONE COPY TO EACH OF THE FOLLOWING PEOPLE:

NAVAL RESEARCH LABORATORY
WASHINGTON, D.C. 20375
- DR. P. MANGE - CODE 4101
- DR. R. MEIER - CODE 4141
- DR. E. SZUSZCZEWICZ - CODE 4187
- DR. J. GOODMAN - CODE 4180
- DR. R. RODRIGUEZ - CODE 4187
- CODE 2628 - 20CY

A.F. GEOPHYSICS LABORATORY
L.G. HANSCOM FIELD
BEDFORD, MA 01730
- DR. T. ELKINS
- DR. W. SWIDER
- MRS. R. SAGALYN
- DR. J.M. FORBES
- DR. T.J. KENESHEA
- DR. J. AARONS
- DR. H. CARLSON
- DR. J. JASPERSE

CORNELL UNIVERSITY
ITHACA, NY 14850
- DR. W.E. SWARTZ
- DR. R. SUDAN
- DR. D. FARLEY
- DR. M. KELLEY

HARVARD UNIVERSITY
HARVARD SQUARE
CAMBRIDGE, MA 02138
- DR. M.B. McELROY
- DR. R. LINDZEN

INSTITUTE FOR DEFENSE ANALYSIS
400 ARMY/NAVY DRIVE
ARLINGTON, VA 22202
- DR. E. BAUER

MASSACHUSETTS INSTITUTE OF TECHNOLOGY
PLASMA FUSION CENTER
LIBRARY, NW16-262
CAMBRIDGE, MA 02139

NASA
GODDARD SPACE FLIGHT CENTER
GREENBELT, MD 20771
- DR. S. CHANDRA
- DR. K. MAEDA
- DR. R.F. BENSON

NATIONAL TECHNICAL INFORMATION CENTER
CAMERON STATION
ALEXANDRIA, VA 22314
- 12CY ATTN TC

COMMANDER
NAVAL AIR SYSTEMS COMMAND
DEPARTMENT OF THE NAVY
WASHINGTON, D.C. 20360
- DR. T. CZUBA

COMMANDER
NAVAL OCEAN SYSTEMS CENTER
SAN DIEGO. CA 92152
- MR. R. ROSE - CODE 5321

NOAA
DIRECTOR OF SPACE AND ENVIRONMENTAL LABORATORY
BOULDER, CO 80302
- DR. A. GLENN JEAN
- DR. G.W. ADAMS
- DR. D.N. ANDERSON
- DR. K. DAVIES
- DR. R. F. DONNELLY

OFFICE OF NAVAL RESEARCH
800 NORTH QUINCY STREET
ARLINGTON, VA 22217
- DR. G. JOINER

PENNSYLVANIA STATE UNIVERSITY
UNIVERSITY PARK, PA 16802
- DR. J.S. NISBET
- DR. P.R. ROHRBAUGH
- DR. L.A. CARPENTER
- DR. M. LEE
- DR. R. DIVANY
- DR. P. BENNETT
- DR. F. KLEVANS

PRINCETON UNIVERSITY
PLASMA PHYSICS LABORATORY
PRINCETON, NJ 08540
DR. F. PERKINS

SCIENCE APPLICATIONS, INC.
1150 PROSPECT PLAZA
LA JOLLA, CA 92037
DR. D.A. HAMLIN
DR. L. LINSON
DR. E. FRIEMAN

STANFORD UNIVERSITY
STANFORD, CA 94305
DR. P.M. BANKS

U.S. ARMY ABERDEEN RESEARCH
AND DEVELOPMENT CENTER
BALLISTIC RESEARCH LABORATORY
ABERDEEN, MD
DR. J. HEIMERL

UNIVERSITY OF CALIFORNIA,
BERKELEY
BERKELEY, CA 94720
DR. M. HUDSON

UNIVERSITY OF CALIFORNIA
LOS ALAMOS SCIENTIFIC LABORATORY
J-10, MS-664
LOS ALAMOS, NM 87545
M. PONGRATZ
D. SIMONS
G. BARASCH
L. DUNCAN
P. BERNHARDT

UNIVERSITY OF CALIFORNIA,
LOS ANGELES
405 HILLGARD AVENUE
LOS ANGELES, CA 90024
DR. F.V. CORONITI
DR. C. KENNEL
DR. A.Y. WONG

UNIVERSITY OF MARYLAND
COLLEGE PARK, MD 20740
DR. K. PAPADOPOULOS
DR. E. OTT

UNIVERSITY OF PITTSBURGH
PITTSBURGH, PA 15213
DR. N. ZABUSKY
DR. M. BIONDI
DR. E. OVERMAN

UTAH STATE UNIVERSITY
4TH AND 8TH STREETS
LOGAN, UTAH 84322
DR. R. HARRIS
DR. K. BAKER
DR. R. SCHUNK

*U.S. GOVERNMENT PRINTING OFFICE: 1982 361-334/555 1-3